INFORMATION TO USERS

This manuscript has been reproduced from the microfilm master. UMI films the text directly from the original or copy submitted. Thus, some thesis and dissertation copies are in typewriter face, while others may be from any type of computer printer.

The quality of this reproduction is dependent upon the quality of the copy submitted. Broken or indistinct print, colored or poor quality illustrations and photographs, print bleedthrough, substandard margins, and improper alignment can adversely affect reproduction.

In the unlikely event that the author did not send UMI a complete manuscript and there are missing pages, these will be noted. Also, if unauthorized copyright material had to be removed, a note will indicate the deletion.

Oversize materials (e.g., maps, drawings, charts) are reproduced by sectioning the original, beginning at the upper left-hand corner and continuing from left to right in equal sections with small overlaps. Each original is also photographed in one exposure and is included in reduced form at the back of the book.

Photographs included in the original manuscript have been reproduced xerographically in this copy. Higher quality 6" x 9" black and white photographic prints are available for any photographs or illustrations appearing in this copy for an additional charge. Contact UMI directly to order.

UMI

A Bell & Howell Information Company
300 North Zeeb Road, Ann Arbor MI 48106-1346 USA
313/761-4700 800/521-0600

DYNAMICS OF GRAVITY WAVES

A dissertation submitted to the

Division of Research and Advanced Studies

of the University of Cincinnati

in partial fulfillment of the

requirements for the degree of

DOCTOR OF PHILOSOPHY

in the Department of Physics

of college of Arts and Sciences

1996

Xuerong Li

B. S. Jilin University (P. R. China) 1983

M. S. Jilin University (P. R. China) 1987

Committee Chair: Dr. Tai Fu Tuan

UNIVERSITY OF CINCINNATI

November 15, 19 96

I, Xuerong Li,
hereby submit this as part of the requirements for the degree of:

Doctor of Philosophy

in Physics

It is entitled Dynamics of Gravity waves

Approved by:

Tai-Fu Feng

Thomas E. Kinnell

H. Gleiche

[illegible]

Abstract

This paper consists of three parts. Part I is gravity wave growth, saturation and decay with height; part II reflection of gravity waves from critical layer using realistic background atmosphere and background wind; part III perturbation treatment of minor species' response to gravity waves. In part I by using Newtonian cooling and Rayleigh friction approximations and by considering only the average effects of turbulence on gravity waves we have derived an optical potential, with which we have studied the propagation of gravity waves and their reflections at every height level. We have found that reflections from higher level due to viscosity and heat conduction is so small that no ducting can be sustained. part II is the continuation of He Fan's work. In our work we adopt the same two parameter optical potential to model the gravity wave - critical layer interaction but we relaxed the conduction of isothermalness of the background and the linearity of the wind profile and we use the more realistic wind models, so our results should be more meaningful. We have found that the reflection coefficients of gravity waves from critical layer range from 5% to 25%, which should be measurable. In part III we develop a perturbation scheme with which it is possible to calculate the minor species response to any order in the linear gravity wave, including a secular component of the response which leads to wave-induced diffusion of minor species. Calculations to third order over a wide range of wave parameters show that the nonlinear effects can be substantial. A result is that care must be taken when analyzing data from minor species fluctuations, so that frequencies due solely to the nonlinear nature of the minor species response are not attributed to gravity waves.

Acknowledgment

First I would like to thank my thesis advisor, Dr. Tai Fu Tuan, for his academic nourishment, guidance and encouragement. I am glad to have him as my mentor.

I thank Dr. H. Fenichel, Dr. Y. Kim and J. Russell for serving in my thesis committee and for their constructive criticism.

I thank the faculty, staff and fellow students at the physics department of the university of Cincinnati for their help.

I thank Dr. J. Isler for informative discussions and enjoyable collaborations in one part of my thesis. I also thank Dr. F. He for his help.

Finally I would like to thank my family for their constant support, encouragement and understanding. A special thanks go to my wife, Jiangyan Lou, for her sacrifice over the years.

Table of Contents

List of Figures

PART I - Gravity wave growth, saturation and decay with height

1. Introduction

Gravity waves of atmosphere have been under study for more than three decades. Gravity waves and their effects are present in the upper and middle atmospheres at all times and in all geographic locations, which are demonstrated by the irregular winds in the upper atmosphere. The propagation and attenuation of gravity waves have important consequences on the whole atmosphere. The vertically propagating gravity wave grows in amplitude exponentially as $\rho_o^{-1/2}$ (where ρ_o is the basic unperturbed pressure), and at some height reach amplitudes for which the wave fields themselves would be strongly unstable (i. e., the combination of mean and wave fields would produce a Richson number below 0.25). Above such height the gravity wave will generate sufficient turbulence, on the average, to prevent further wave growth with height. This phenomenon is called wave breaking or saturation, which was noted by Lindzen [1,2] and Hodges [3] for tides and gravity waves in the mesosphere. It was estimated by Lindzen and Blake [4] that gravity wave breaks down between 80 and 90 km, generating turbulence which prevents wave from growing. Molecular viscosity and conductivity become more and more important with height. Above 110 km, the amplitude of upward gravity wave will decrease into viscosity and conductivity.

The purpose of this paper is to investigate the behavior of the gravity wave and its reflection at every height level with the optical model, in

which we use optical potential to take care of the dissipative losses from heat conduction, viscosity and turbulence. We linearize the equations of motion of atmosphere with heat conduction and molecular viscosity. By making Newtonian Cooling and Rayleigh friction approximations, we convert the linearized equations into a second order Sturm-Liousville equation. Turbulence is purely due to nonlinearity which is hard to deal with. In this scheme we only consider the average effect of turbulence on gravity wave by the introduction of a phenomenological optical potential, which will exactly offset the exponential growth of gravity wave in the isothermal atmosphere. In this part we make the following assumptions:

(a) the background atmosphere is quiet, time-independent and vertically stratified, i.e., all unperturbed quantities depend only on the vertical coordinate (z)

(b) the rotation of the earth may be neglected

(c) the Boussinesq approximation

(d) the curvature of the earth is neglected.

Based on the above assumptions and the optical model. We gets some interesting results:

(1) the viscosity loss is just as important as the heat conduction loss throughout the atmosphere contrary to some views;

(2) the variation of most losses are slow enough so that the principal agent for wave reflection is due to background structure;

(3) the dissipative losses tend on the whole to reduce wave reflection rather enhancing it;

(4) gravity wave saturation tends to be more readily identifiable in the larger scale gravity waves.

2. Equations

The hydrodynamic equations without approximations are the equation of continuity:

$$\frac{\partial \rho}{\partial t} + \nabla \cdot (\rho \vec{v}) = 0 \tag{1}$$

the equation of momentum conservation

$$\rho \frac{\partial \vec{v}}{\partial t} + \rho \vec{v} \cdot \Delta \vec{v} = -\nabla \rho + \vec{g} - \Delta \cdot \bar{\bar{S}} \tag{2}$$

the equation of energy conservation

$$\frac{1}{\gamma - 1}\left[\frac{\partial T}{\partial t} \vec{v} \cdot \nabla T\right] = \nabla(\lambda \nabla T) - p(\nabla \cdot \vec{v}) + \bar{\bar{S}} : \bar{\bar{\wedge}} \tag{3}$$

The state equation

$$p = \frac{k_b}{m} pT \tag{4}$$

where

$$S_{ij} = \frac{1}{2}\left(\frac{\partial v^i}{\partial x_j} + \frac{\partial v_i}{\partial x^j}\right) - \frac{2}{3}\delta_{ij} \nabla \cdot \vec{v} \tag{5}$$

$$\wedge^{ij} = \frac{1}{2}\left(\frac{\partial v^i}{\partial x_j} + \frac{\partial v^j}{\partial x_i}\right) \tag{6}$$

$\vec{v}$ is the velocity, p is the pressure, c is the speed of sound, $\vec{g}$ is the acceleration due to gravity, k is the heat conduction coefficient, and μ is viscosity. Because of the assumption that the rotation of the earth can be neglected it well known that the problem becomes two dimensional; x-direction defined by the horizontal wind and the vertical z-direction. We assume that the perturbation quantities Δf (x, z, t) can be decomposed into monochromatic plane waves as given by

$$\Delta f(x,z,t) = \tilde{f}(z)e^{i(\omega t - k_x x)} \tag{7}$$

ω is angular frequency and k_x wave vector.

To simplify, we use Newtonian cooling and Rayleigh Friction approximations, i.e.,

$$\nabla \cdot (\lambda \nabla T) \approx -bT \tag{8}$$

$$\nabla \cdot \bar{\bar{S}} \approx -d\vec{v} \tag{9}$$

Where the b and d are constants. The linearized equations are:

$$i\omega\Delta\rho = ik_x\rho_0\Delta u - \frac{\partial}{\partial z}(\rho_0\Delta w) \tag{10}$$

$$i\omega\rho_0\Delta u = ikx\Delta p - d\Delta u \tag{11}$$

$$i\omega\rho_0\Delta w = -g\Delta\rho - \frac{\partial}{\partial z}(\Delta p) - d\Delta w \tag{12}$$

$$\frac{\rho_0 k}{(\gamma-1)m}\left(i\omega\Delta T + \frac{\partial T_a}{\partial z}\Delta w\right) = -b\Delta T + ik_x p_0\Delta u - p_a\frac{\partial(\Delta w)}{\partial z} \tag{13}$$

$$\Delta p = \frac{k_b}{m}(\rho_0\Delta T + T_0\Delta\rho) \tag{14}$$

defining renormalized pressure and vertical velocity variations as:

$$\psi = \frac{\omega\Delta p}{\sqrt{\rho_0}} \tag{15}$$

$$\phi = \omega\sqrt{\rho_0}\Delta w \tag{16}$$

Eliminating the density perturbation δp and horizontal particle velocity δu from Eqs (10)-(14) we obtain

$$\phi' = -\frac{1}{2}\frac{\rho'_0}{\rho_0}\phi - i\omega\left[\frac{\gamma}{c^2} - \frac{k_x^2}{\omega^2}\right]\psi + \frac{i\omega^2\rho_0^{1/2}\gamma k_m}{c^2}\Delta T \tag{17}$$

$$\psi' = -i\omega\Phi - \left[\frac{g\gamma}{c^2} + \frac{1}{2}\frac{\rho_0^2}{\rho_0}\psi + \frac{\omega g\rho_0^{1/2}\gamma k_m}{c^2}\right]\Delta T \tag{18}$$

$$\left(i\omega\frac{\rho_0 k_m}{\gamma-1} + \lambda\left(k_x^2+k_z^2\right)\right)\Delta T = -i\frac{k_x^2c^2}{\omega^2\gamma}\rho_0^{1/2}\Psi - \frac{1}{2}\frac{c^2}{\gamma}\frac{\rho'_0}{\rho_0^{1/2}}\frac{\Phi}{\omega} + \frac{c^2}{\gamma\omega}\rho_0^{1/2}\Phi' + \frac{\rho_0^{1/2}}{\omega\gamma(\gamma-1)}\frac{\partial c^2}{\partial z}\Phi \tag{19}$$

Combining Eqs (17) and (19) yields

$$\Delta T = \frac{1}{i\omega \frac{\rho_0 k_m \gamma}{\gamma - 1} + \lambda\left(k_x^2 + k_z^2\right)}\left[i\rho_0^{1/2}\Psi + \frac{c^2 \rho'_0}{\gamma\omega\rho_0^{1/2}}\phi - \frac{\rho_0^{1/2}}{\omega\gamma(\gamma-1)}\frac{\partial c^2}{\partial z}\Phi \right] \tag{20}$$

Eliminating temperature perturbation ΔT yields

$$\Psi' = -i\omega\left[\frac{\alpha g}{\omega^2 \gamma c^2}\frac{\partial c^2}{\partial z} - \frac{\alpha g(\gamma-1)\rho'_0}{\omega^2\gamma\rho_0} - 1\right]\phi + \left[\frac{g(\alpha g(\gamma-1)-\gamma)}{c^2} - \frac{1}{2}\frac{\dot{\rho_o}}{\rho_0}\right]\psi \tag{21}$$

$$\Phi' = \left[\left(\frac{\partial(\gamma-1)}{\gamma} - \frac{1}{2}\right)\frac{\rho'_0}{\rho_0} - \frac{\alpha}{\gamma c^2}\frac{\partial c^2}{\partial z}\right]\Phi + i\omega\left[\frac{\alpha(\gamma-1)-\gamma}{c^2} + \frac{k_x^2}{\omega^2}\right]\Phi \tag{22}$$

By eliminating ϕ, we get

$$\frac{d^2\Psi}{dt} + p\frac{\Psi}{dt} + q\Psi = 0 \tag{23}$$

where

$$p = J + M - \frac{N'}{N} \tag{24}$$

$$q = M' + NK + M\frac{N'}{N} + MJ \tag{25}$$

and

$$M = -\frac{\left[\alpha g(\gamma-1)-\gamma\right]}{c2} + \frac{1}{2}\frac{\rho'_0}{\rho_0} \tag{26}$$

$$N = \omega\left[\alpha\frac{\omega_b^2}{\omega^2} - (1 - id_1)\right] \tag{27}$$

$$J = -\left(\alpha - \frac{1}{2}\right)\frac{\dot{\rho}_0}{\rho_0} - \frac{\alpha g}{c^2} \tag{28}$$

$$k = \omega\left[\frac{\alpha g(\gamma - 1) - \gamma}{c^2} + \frac{k_x^2}{\omega^2(1 - id_1)}\right] \tag{29}$$

with

$$\alpha = 1 - i\beta \tag{30}$$

$$\beta = \frac{b(\gamma - 1)m}{\omega \rho_o k} \tag{31}$$

$$d_1 = \frac{d}{\rho_o \omega} \tag{32}$$

Thus, both α and β provide a measure of heat conduction whilst d_1 provides a measure of viscosity.

To determine b and d explicitly in terms of a WKB formulation:

$$b\Delta T = -\nabla \cdot [\lambda \nabla(\Delta T)]$$

$$= -\lambda\left(\frac{\partial^2(\Delta T)}{\partial x^2} + \frac{\partial^2(\Delta T)}{\partial z^2}\right)$$

$$\approx \lambda(k_x^2 + k_z^2) \tag{33}$$

We obtain

$$b \approx \lambda(k_x^2 + k_z^2) \tag{34}$$

$$d\Delta\vec{v} \approx \nabla \cdot \vec{s}$$

$$= \hat{e}_x \mu[-(\frac{4}{3}k_x^2 + k_z^2)\Delta u - \frac{1}{3}k_x k_z \Delta w] + \hat{e}_3 \mu[-\frac{4}{3}k_z^2 + k_x^2)\Delta w - \frac{1}{3}k_x k_z \Delta u]$$

$$d \approx \frac{4}{3}k_z^2 + k_x^2 \tag{35}$$

Here we neglect the cross terms and assume the same given by the above. Turbulence is due to nonlinearity which is hard to handle. To model its effect, people usually adopt linear scheme. For example, the introduction of turbulent viscosity to model turbulence is one of such an attempt. In this paper we use another linear scheme by introducing a phenomenological optical potential to model its effects on gravity waves. The interactions between turbulence and other dissipative losses such as heat conduction and viscosity is very small, which can be ignored safely. In saturation region, the turbulence just cancels the exponential growth of upgoing linear gravity wave. Therefore, the amplitude of gravity wave stays more or less the same. Based on this observations, we can get the analytical form of phenomenological optical potential for turbulence in the isothermal case. Without turbulence in isothermal background

$$\Psi'' + k_z^2 \Psi = 0 \tag{36}$$

where k_z is a real number. With turbulence, the equation becomes

$$\Psi'' + (k_z^2 - V_t - iW_t)\Psi = 0 \tag{37}$$

The normalized pressure must decay exponentially as $e^{-\frac{k_z z}{2H}}$ to produce saturation, from which we get

$$V_t = \frac{1}{4H^2} \tag{38}$$

$$W_t = \frac{k_z}{H} \tag{39}$$

Where H is atmospheric scale height. We simply generalize the above potential to the real atmosphere without any modification. The full equation with turbulence is

$$\Psi'' + p\Psi' + [q - f(V_t + W_t)\Psi = 0 \tag{40}$$

where $0 \le f \le 1$. f is a parameter. f = 0 means no turbulence and f = 1 full turbulence.

Reflection Coefficient

We assume that there exists a very narrow vertical strip of locally isothermal region in which we can define an upgoing and downgoing wave with a reflection coefficient as well as a local wave vector. Namely,

$$F(z) = A(\underline{z})e^{ik(z-\underline{z})} + B(\underline{z})e^{-ik(z-\underline{z})} \tag{41}$$

From it we can easily find the reflection coefficient at any position $\underline{z}$

$$R(\underline{z}) = \frac{|B(\underline{z})|}{|A(\underline{z})|} = \left|\frac{ikF(\underline{z}) - F'(\underline{z})}{ikF(\underline{z}) + F'(\underline{z})}\right| \tag{42}$$

with local wave number

$$k = \sqrt{-\frac{F''(\underline{z})}{F(\underline{z})}} \tag{43}$$

In the above derivation we ignore the first order derivative of k, which is very small in our case.

3. Results and discussion

To carry out these calculations, it is necessary to choose some model for the atmosphere. For the atmosphere we choose COSPAR atmospheric model. The kinematic viscosity μ/ρ_0 is plotted in Fig. 3. The viscosity below 70km was taken from the data given by Lettau, but it has been smoothed considerably, and calculation of Colegrove et al was used to determine the value near 100km. Elementary kinetic theory indicates that the molecular thermal kinetic conductivity is related to the molecular viscosity by the formula:

$$\lambda = \frac{\kappa k}{m(\gamma - 1)}\mu \tag{44}$$

where κ is a numerical factor equal to about 1.87 for N_2 and 1.91 for O_2, and 2.57 die O (Dalgarna and Smith, 1962). The specific value used at each

height has been obtained by averaging in accordance with the relative concentrations of these species. In Fig. 1(1-4) we showed the optical potentials along with the gravity waves of various horizontal phase velocities at a fixed period. As can been shown, the optical potential is very sensitive to the horizontal phase velocity. The peak barrier occurs at lower altitude for smaller scale waves and at higher altitude for larger scale gravity waves. Therefore, large scale gravity wave can propagate higher into the atmosphere, which is in agreement with experiment. Fig. 1.15 showed the reflection coefficient varies with altitude for a specific gravity wave. As we can see that the reflection coefficient at low altitude is very large, which is caused overwhelmingly by background structure of atmosphere. Then, it becomes very small. The smallness of reflection coefficient in this region is due to the facts that background is very flat. But when gravity wave goes up higher, reflection coefficient becomes larger and larger because viscosity and heat conduction finally becomes dominant factor. We know that the potential without any loss is very flat in high altitude. Flat potential will not produce any reflection, therefore, reflection at higher altitude is almost entirely due to dissipative losses. Our calculation show that the reflection from dissipative losses is so small that it can not sustain any duction of gravity wave, which is against some people's belief[5]. From Fig.1(4-14) we can see that the turbulence plays less important role for smaller scale gravity wave and becomes more and more important as horizontal wavelength of gravity wave increases. This is easily understandable. Small scale gravity wave get absorbed before saturation while larger scale gravity wave first get saturated, and the absorbed.

3 Conclusions

From the results, we get the following conclusions:

(1) The overall envelope of the growth and decay of the horizontal velocity profile depends much more strongly on the higher kinetic viscosity and heat conduction at higher altitudes. The turbulence plays a relatively minor role.

(2) The effect of saturation is much more clearly shown in the larger scale waves. For the gravity waves with much less horizontal phase velocity than 50 m/s in the shape of the envelope remains the same irrespective of the degree of turbulence and saturation.

(3) The relative insensitivity of the envelope to the presence of turbulence implies that it is not a good tool for determining the degree of turbulence for small scale gravity waves.

(4) The reflection due to both background structure and dissipative loss is very small for small scale gravity waves, although they can be both very large for the larger scale gravity waves. For the medium scale gravity waves the reflection at low altitudes is far higher than higher altitudes.

Part II - Reflection of gravity waves from critical layer using the realistic atmosphere and horizontal wind

1. Introduction

The subject of gravity-wave critical-layer interaction has received much attention[7-13]. In all these papers the attention has been focused on the mechanisms for the interaction and the excitation of new gravity wave modes, very little attention has been paid to the effect of the interaction on the original wave, including the downward reflected wave below critical layer. He Fan et. al. [14] have studied the problem of the gravity wave - critical layer interaction in an isothermal background with a horizontal wind that increases proportionally with height after a certain height. The authors have used a two parameter optical potential to model the gravity - critical layer interaction. In this paper we adopt the same model to study the gravity wave - critical layer interactions in the real atmosphere. It is our purpose to determine the magnitude of this reflection, how it varies with the horizontal phase velocity and direction of propagation of the incident wave.

Much of the previous work on the critical layer has been made use of the WKB approximation [16] for the incident wave, which basically neglects reflections. As the critical layer is approached, the incident wave is absorbed by a large number of mechanisms: (a) frequency broadening due to nonlinear wave growth; (b) turbulence generated by connective instability; (c) dissipation from viscosity and heat conduction; (d)

absorption into the mean flow; (e) excitation of new modes. In view of the fact that all such wave absorption takes place over a vertical distance short compared with the incident vertical wavelength. We would expect from basic physics that the reflections from the critical-layer region should be considerable.

In 1978 Richmond [17] showed that for large-scale gravity waves the wave absorption from viscosity and heat conduction at high altitude can produce so much downward reflection on an upward propagating gravity wave that some degree of gravity-wave ducting can actually occur. In that paper a three-layer model was used to simulate the viscous and heat conduction absorption.

To determine such reflections for different gravity-wave phase velocities and different background winds, we parametrize the above mentioned losses through a single absorption parameter very similar to the optical model [18]. The optical potential treatment has been successfully used in nuclear physics and unsuccessfully in atomic physics, because for the latter the absorption is very structured. Owing to the large variety of mechanisms of dissipation in the critical layer region, the problem in this study bear many similarities to the scattering problems in nuclear physics, and thus the same technique may be used. In nuclear physics, one wants to know what happens to a particular scattering channel (e.g., the elastic channel with no loss of incident energy or the inelastic channel with an excitation of the target nucleus) without having to solve the entire many-body problem which often involves intractable nonlinear field equations. the optical model is then used to replace as much as possible the effects of

the physics of the unwanted-channels on the particular channel of interest. Most important of all, the optical model reduces an intractable nonlinear system to a tractable linear problem which focuses only on one channel. our interest is in setting limits on the reflections of the original incident wave with the original incident wave parameters (i.e. the elastic scattering) produced by gravity-wave and critical-layer interaction which is highly nonlinear. To model the interaction we introduce the optical potential to phenomenologically take care of the myriad of relatively unstructured losses just mentioned. The physical justification for this comes from the narrowness of the vertical range over which the losses occur as compared with the incident vertical wavelength. The optical potential will take care of all the dissipations, which include viscosity, heat conduction, instability, turbulence and newly created modes.

We use the method of [13] for computing the width of the instability region, which is small compared with the average vertical wavelength of the incident gravity wave. due to the relative long wavelength, the exact functional form of the potential no longer matters and we choose two parameter potential, namely the strength (labeled Wo) and the range of the optical potential. as the range can be estimated the only free parameter left then is Wo. we shall vary this parameter to give us a range of reflection coefficients and we will show that the actual reflection from the critical level itself plays almost no role for most reasonable values of Wo.

In our calculation we use COSPAR atmospheric models with NCAR-CEDAR [18] wind profiles modified by the tidal-wave model of [19]. Because of the singularity of critical layer, any numerical calculation will

fail in that region. But since the instability region is very small compared with the variation in the background atmosphere, as a good approximation we can assume that the background is isothermal within the instability region. this approximation leads to analytic solutions to the linearized hydrodynamic equations. we join the analytical solution to the numerical solution at the lower end of the instability region. Once the gravity-wave solutions have been determined, the solutions can be used to compute the reflection coefficients and the response of airglow to a gravity-wave in the presence of critical layers. That the critical layers may have a strong effect on gravity-wave propagation has already been show through the airglow observations of [20] based on the "blocking diagrams" of [21]. Our wish is to construct a gravity-wave model in the presence of critical layer.

Based on our study we can conclude that (1) with any reasonable absorption from nonlinearity and turbulence and for stable background wind, most of the reflection and absorption takes place before the wave reaches the critical level and the fraction of gravity-wave which reaches critical layer is very small and therefore the total reflection from the critical-layer region is in fact independent of the reflection parameter at critical-layer region is in fact independent of the reflection parameter at critical level. (2) the gravity-wave critical layer interaction in the presence of an unstable wind can result in wave emission and growth rather than wave absorption. Thus instead of a "sink" for absorbing gravity waves, critical layer becomes a "source" for creating gravity waves. In such case the reflection coefficient is greater than unity and over-reflection can occur [22]. (3) there are some resonance absorption states in which the reflections from critical layer and from background interfere destructively.

2 Mathematical Formulation

The linearized hydrodynamic equations in the presence of horizontal winds [23] are given by:

$$\frac{d\psi}{dz} - \eta\psi = \frac{i}{\omega}(\omega_b^2 - \Omega^2)\Phi \qquad (1)$$

$$\frac{d\Phi}{dz} + (\eta + \frac{\kappa_h}{\Omega}\frac{\partial V_o}{\partial z})\phi = i(\frac{\kappa_h}{\Omega^2} - \frac{1}{c^2}) \qquad (2)$$

where

ω= observed gravity-wave frequency

v_h= horizontal phase velocity

$\omega_b = -g(\frac{1}{p_o}\frac{dp_o}{dz} + \frac{g}{c^2})$

$\Psi = \frac{\omega\Delta\rho}{\rho_o^{1/2}}$ = pressure variation, Δ_ρ, normalized to include the background density variation

$\Phi = \rho_o^{1/2}\omega\Delta\omega$= vertical velocity variation, $\Delta\rho$, also normalized in a similar way

$\Omega = \omega - \vec{\kappa}_h \bullet \vec{V}_o = \omega - \kappa_h V_o = \omega\left(1 - \frac{V_o}{V_h}\right)$= intrinsic Doppler shifted frequency

$\vec{\kappa}$= wave vector (κ_h =its horizontal component)

v_o = horizontal background velocity

$\eta = -\left(\frac{1}{2}\frac{1}{\rho_o}\frac{dp_o}{dz} + \frac{g}{c^2}\right)$

An oscillatory factor, $\exp(i\omega t - ik_h x)$ is dropped out of Ψ and Φ in all equations. The coupled equations given by (1) and (2) can be combined to yield

$$\frac{d}{dz}\left(\frac{1}{\omega_b^2-\Omega^2 dz}\right)-\left[\frac{d}{dz}\left(\frac{\eta}{\omega_b^2-\Omega^2}\right)+\frac{\eta^2}{\omega_b^2-\Omega^2}+\frac{1}{c^2}-\frac{\kappa_x^2}{\Omega^2}\right]\Psi=0 \qquad (3)$$

We will use numerical method in finding the gravity-wave solutions to equation (3). But in the vicinity of the critical level equation (3) becomes singular, and the numerical method can not apply. To solve this problem we assume that the back-ground around the critical level is isothermal and use analytical solutions which can then be joined to the numerical solutions outside the critical-layer region. Since the instability region ranges from several hundred meters to a couple of kilometers for most gravity waves of interest, the background temperature may be assumed to be isothermal over such a short vertical region. with this assumption, the equation (3) in the vicinity of critical layer becomes

$$\frac{d}{dz}\frac{1}{1-x^2}\frac{d\Psi}{dx}+\left[\frac{\lambda}{x^2}-\frac{\sigma^2}{1-x^2}+\frac{2\sigma x}{\left(1-x^2\right)^2}-\nu\right]\Psi=0 \qquad (4)$$

where

$x=\frac{\Omega}{\omega_b}$ the new coordinate introduced; x=0 corresponds to $\Omega=0$ where the critical layer occurs, and x is positive going downwards.

$\mu=\frac{\omega_b^4}{h_h^2\beta^2c^2}$ = eigenvalue (dimensionless)

$\sigma=\frac{\omega_b\eta}{\kappa_h\beta}$

$\lambda=\frac{\omega_b^2}{\beta^2}$ = background Richardson number (dimensionless)

$\beta=\frac{\partial V_o}{\partial z}$ = wind gradient

By multiplying (5) from the left by Ψ^* and the Hermitian adjoint of (4) by Ψ, subtracting the latter from the former and integrating from x=a to x=b, where a and b are two arbitrary positions, we obtain:

$$\left[\Psi^* \frac{1}{1-x^2}\frac{d\Psi}{dx} - \Psi \frac{1}{1-x^2}\frac{d\Psi^*}{dx}\right]_a^b = 0 \qquad (5)$$

Equation (5) holds because the eigen value of a Sturm-Liouville equation is real. Since a and b are arbitrary positions, we conclude:

$$\Psi^* \frac{1}{1-x^2}\frac{d\Psi}{dx} - \Psi \frac{1}{1-x^2}\frac{d\Psi^*}{dx} = \text{constant} \qquad (6)$$

Multiplying (1) from the left by $\Psi^*/(1-x^2)$ and its Hermitian adjoint by $\Psi/(1-x^2)$ and subtracting the latter from the former, we obtain:

$$\Psi^* \frac{1}{1-x^2}\frac{d\Psi}{dx} - \Psi \frac{1}{1-x^2}\frac{d\Psi^*}{dx} = \frac{-i\omega_b^2 v_h^2}{\beta}\frac{\left(\Delta p^* \Delta\omega + \Delta p \Delta\omega^*\right)}{v_h - V_o} \qquad (7)$$

In equation (7) we have used the fact that

$$\Psi^*\Phi = \omega^2 \Delta p^* \Delta w$$
$$\Psi\phi^* = \omega^2 \Delta p \Delta w^* \qquad (8)$$

From equation (7) we obtain:

$$\Psi^* \frac{1}{1-x^2}\frac{d\Psi}{dx} - \Psi \frac{1}{1-x^2}\frac{d\Psi^*}{dx} = -\frac{4i\omega_b^3 v_h^2}{\beta}\frac{\langle \Delta p^* \Delta w \rangle}{v_h - V_o} \qquad (9)$$

where the bracket term on the right is the time-averaged vertical energy flux. From (6) the left hand side of equation (9) is constant, we come to the conclusion that:

$$\frac{\langle \Delta p^* \Delta w \rangle_t}{v_h - V_o} = \text{constant} \tag{10}$$

Equation (10) states that the vertical energy flux of the gravity wave divided by the difference between its horizontal phase velocity and the horizontal wind velocity along the propagation direction remains a constant. This can be recognized as a direct consequence of the Eliasson and Palm theorems for an inviscid atmosphere where the only loss of energy from the gravity wave is mean flow.

So far our mathematical formulation has described only the loss mechanism (d), the absorption into the mean flow. We will not consider mechanism (c), since dissipation from viscosity and heat conduction are very small [1] except very close to the critical level where their effects will be modeled by a complex parameter, R_c, the "reflection" coefficient at the critical level. the other loss mechanisms including the important instability and turbulence will be described phenomenologically by incorporating an optical potential in (4).

In the present treatment the vertical wave length of the incident gravity wave is typically of the order of low tens of kilometers, while the vertical range of the region in which the gravity wave is nonlinear and the atmosphere is convectively unstable is of the order of only a couple of

kilometers[12]. thus, the effective range over which strong absorption occurs is considerably less than the wavelength of the incident gravity wave. From basic scattering theory this means that the scattering and hence the reflection from the strongly interaction region is relatively independent of the "shape" of the optical model 'potential" and the entire scattering process can be described by s simple two-parameter optical "potential".

We will allow our choice to be guided by the worst-case scenario, that is the most singular behavior at the critical layer, which arises from the nonlinear convective derivative term in the momentum equation. to lowest order, this term is given by

$$\rho\left(\vec{v}\cdot\vec{\Delta}\right)\vec{v} \approx K\frac{\Psi}{x^2} \qquad (11)$$

where K is an a dimensional constant. The expression (5) is obtained by substituting the linear solution for v and p on the left of (5) and using the known behavior of [13] near the critical level. Thus we may choose the following optical potential:

$$V_{optical} = \frac{iW_o}{x^2} \qquad (x < x_m)$$

$$V_{optical} = 0 \qquad x > x_m \qquad (12)$$

where Wo is negative for wave absorption and provides a measure for the potential depth. x_m corresponding to z_m is the position where the instability begins and 0- x_m provides a measure for the range over which the absorption is active. Wo and x_m constitute the two parameters of our

model. However, as will be shown in the next section, x_m can be individually determined.

Using the optical model as an absorption mechanism [13], we incorporate this mechanism purely phenomenologically by adding optical potential to the real potential in (4) to obtain

$$\frac{d}{dx}\frac{1}{1-x^2}\frac{d\Psi}{dx}+\left[\frac{\lambda+iWo}{x^2}-\frac{\sigma^2}{1-x^2}+\frac{2\sigma x}{\left(1-x^2\right)}-\nu\right]\Psi=0 \qquad (13)$$

Since $x_m \ll 1$, in the region of $0<x<x_m$ the analytic solution to the lowest order is good enough for our purpose. The solution to (7) depends on whether the background wind profile is stable $(\lambda > 1/4)$ or unstable $(\lambda < 1/4)$. At any arbitrary but fixed location, $x=\underline{x}$, we can find plane wave solutions in the immediate vicinity of $\underline{x}$, i.e., $x=\underline{x}+\delta$ where $\delta/\underline{x} \ll 1$[1]. We list the solutions to the lowest order in x in table I for $0< x < x_m$.

Table I

	$\lambda > 1/4$	$\lambda < 1/4$
Ψ_+	$x^{1/2+\bar{\beta}/2}e^{i(-\bar{\alpha}\log_e x)/2}$	$x^{1/2-\bar{\beta}/2}e^{i(\bar{\alpha}\log_e x)/2}$
	$x^{1/2+\bar{\beta}/2}e^{i(-\bar{\alpha}\log_e x)/2}e^{-ik\delta}$	$x^{1/2-\bar{\beta}/2}e^{i(\bar{\alpha}\log_e x)/2}e^{ik\delta}$
Ψ_-	$x^{1/2-\bar{\beta}/2}e^{i(\bar{\alpha}\log_e x)/2}$	$x^{1/2+\bar{\beta}/2}e^{-i(\bar{\alpha}\log_e x)/2}$
	$x^{1/2-\bar{\beta}/2}e^{i(\bar{\alpha}\log_e x)/2}e^{ik\delta}$	$x^{1/2-\bar{\beta}/2}e^{i(\bar{\alpha}\log_e x)/2}e^{-ik\delta}$

where

$$\bar{\alpha}=\left[(4\lambda-1)^2+16W_0^2\right]^{1/4}\cos\left(\frac{\phi}{2}\right)$$

$$\bar{\beta}=\left[(4\lambda-1)^2+16W_0^2\right]^{1/4}\sin\left(\frac{\phi}{2}\right)$$

$$\phi = \tan^{-1}\frac{4W_0}{4\lambda - 1}$$

k=$\left(\frac{\alpha}{2\underline{x}}\right)$=instantaneous wave vector at x=$\underline{x}$

Ψ_+=upgoing (energy) wave

Ψ_-=downgoing (energy) wave

In table I, the top line for each row gives solutions for $\lambda > 1/4$ and $\lambda < 1/4$. The bottom line of each row gives the leading term in the expansion of these solutions about any arbitrary but fixed $\underline{x}$. We see right away that the instantaneous vertical wavelength ($\approx 2\pi/k$) goes to zero as $\underline{x} \to 0$ at the critical point as is well known.

The behavior of upgoing and downgoing waves depend entirely on the argument, ϕ, of the cosine/sine function appearing in $\bar{\alpha}$ and $\bar{\beta}$ for stable and unstable background winds. Fig 1 shows the argument, ϕ. W_0 is always less than zero, we see that for stable background winds ($\lambda > 1/4$), ψ, the argument for the arctangent function, is in the 4th quadrant and therefore for stable background winds $\bar{\alpha}>0$ and $\bar{\beta}>0$. In the limit as W_0 goes to zero, ϕgoes to 2π, $\bar{\alpha}=(4\lambda-1)^{1/2}=\mu$ and $\bar{\beta}=0$. For unstable background winds ($\lambda < 1/4$) and ϕ, the argument for the arctangent, is in the 3rd quadrant, and thus, $\bar{\alpha}>0$ and $\bar{\beta}>0$. In the limit as Wo goes to zero, ϕgoes to π, $\bar{\alpha}$ goes to zero and $\bar{\beta}$ goes to $(1-4\lambda)^{1/2}$.Thus, for stable background winds k>0 and since x is positive going downwards, $\exp[-ik\delta]$ is downward in phase progression and hence upwards in energy propagation. By the same argument, $\exp[ik\delta]$ is upwards in phase progression and downwards in energy propagation. the reverse is true for unstable background wind for which k<0.

The most interesting phenomenon occurs for the case of unstable background winds when becomes negative. We can set $4\lambda - 1 = -e = 1(4\lambda' - 1)$ where $\lambda < 1/4$, e>0, and $\lambda' > 1/4$. Thus

$$\tan\phi = \frac{4W_0}{4\lambda' - 1} = \frac{-4W_0}{e} = \frac{-4W_0}{4\lambda' - 1} \tag{14}$$

This means that an unstable background wind with a negative optical potential, Wo<0, is equivalent to a stable background wind with a positive optical potential, Wo. In this way, instead of an absorbing potential which acts as a sink and takes energy out of the gravity wave, we now have a source which puts energy into the gravity wave. The reflection coefficient is greater that unity and over-reflection occurs. When this happens, the ultimate source of energy is, of course, the background wind.

We now investigate the explicit behavior of the constant in the Eliassen and Palm Theorems given by equation (10). By substituting the lowest order solutions of equation (4) into the left-hand side of equation (9), we obtain for $x \ll 1$:

$$\langle \Delta p \Delta w \rangle_t = \frac{|A|^2 \mu \left(1 - |R_c|^2\right)}{4\lambda^{1/4} \omega \omega_b v_h} x \tag{15}$$

for stable background winds and

$$\langle \Delta p \Delta w \rangle_t = \frac{|A|^2 \bar{\mu} |R_c| \sin\chi}{2\lambda^{1/4} \omega \omega_b v_h} x \tag{16}$$

for unstable background winds. Here A is the wave amplitude for Ψin (15) and (16), $\bar{\mu}=(1-4\lambda)^{1/2}$ in (16) and R_c is the complex reflection parameter at he critical level given by

$$R_c = |R_c| e^{i\chi}$$

From equation (14), we see that over-reflection can occur only if $\chi<0$. We see that over-reflection can occur only if χ has such value that sin $\chi<0$. We also note that for stable background wind

$$R_c = 1 \rightarrow \langle \Delta p \Delta w \rangle_t = 0$$

This merely means that with perfect reflection at the critical level, a standing wave along the vertical direction is produced and the net pressure energy flux is zero.

Important points of interest in (15) and (16) are that the time averaged energy flux depends on : (1) the steepness of the vertical wind gradient; (2) the period of the gravity wave (the greater the period, the greater the absorption into the mean flow); (3) the inverse of horizontal phase velocity (the smaller scale gravity waves are absorbed more) and (4) the altitude (larger Brunt periods at higher altitude mean that the absorption into the mean flow increases with altitude).

With a nonvanishing W_0, we proceed in a similar fashion for the derivation of (9), but start from equation (13) rather equation (4). the result is

$$\Psi^* \frac{1}{1-x^2}\frac{d\Psi}{dx} - \Psi \frac{1}{1-x^2}\frac{d\Psi^*}{dx} + 2iW_0F(x) = const\tan t = iN \qquad (17)$$

where

$$F(x) = \int^x \frac{|\Psi|^2}{x'}dx$$

and

$$N - 2W_0F(x) = \frac{-4\Omega_b^3 v_h^2}{\beta}\frac{\langle \Delta p \Delta w \rangle}{V_h - V_0} \qquad (18)$$

Equation (17) reduces to (9) if W_0=0: and it provides a correction term (i.e. $2\,W_0F(x)$) to the constant N. Equation (18) also provides a generalization to the Eliassen and Palm theorems for the case when there are absorption mechanisms other than into the mean flow.

The same technique used to derived equation (15) and equation (16) can be used to show that (for $x << 1$) with stable background

$$\langle \Delta p \Delta w \rangle_t \approx \frac{\bar{\alpha}|A|^2}{4\lambda^{1/2}\omega\omega_b v_h} x^{1+\bar{\beta}} \qquad (19)$$

and with an unstable background

$$\langle \Delta p \Delta w \rangle_t \approx \frac{\bar{\alpha}|A|^2}{4\lambda^{1/2}\omega\omega_b v_h} x^{1-\bar{\beta}} \qquad (20)$$

In equation (19) and (20), the R.H.S. gives the behavior of the energy flux with its leading term. The reason that the time-averaged energy flux does not vanish for equation (19) as it would have for equation (15) when $|R_c|=1$ is the absorption, W_0. This absorption upsets the balance between the upgoing and downgoing fravity wavees giving us a net energy flux.

The behavior of equations (19) and (20) which include absorption into channels other than just the mean flow is quite different from that of equation (15) and (16) which only allow the absorption into the mean flow. For one thing the numerators on the right hand side of equaitons (19) and (20) do not vanish as λ passes through 1/4. Also, in general, $\langle \Delta p \Delta w \rangle_t$ in equation (19) and (20) depend on the steepness of the wind gradients; the steeper the wind gradient, the greater the net energy flux at any value of x within reasonable distance to the critical level ($x \ll 1$). This is readily uunderstandable since at any fixed location a steeper wind gradient would greatly enhance the instability and turbulence thereby increase that type of loss through a rise in the net energy flux. On the other hand the dependence of $\langle \Delta p \Delta w \rangle$ on Brunt period etc. are the same as for equations (19) and (20). Thus, as x goes to zero the ratio of the energy flux without absorption to the energy flux with absorption is given by:

$$\frac{\langle \Delta p \Delta w \rangle_{w_0=0}}{\langle \Delta p \Delta w \rangle_{w_0 \neq 0}} \rightarrow \frac{\mu\left(1-|R_c|^2\right)}{\bar{\alpha}} x^{-\bar{\beta}} \qquad (21)$$

for stable background wind and by

$$\frac{\langle \Delta p \Delta w \rangle_{w_0=0}}{\langle \Delta p \Delta w \rangle_{w_0 \neq 0}} \rightarrow \frac{2\tilde{\mu}|R_c \sin\chi}{\bar{\alpha}} x^{\bar{\beta}} \qquad (22)$$

for unstable background wind.

Since $\bar{\beta}<0$ for equation (21) and $\bar{\beta}>0$ for equation (22), both ratios vanish as x goes to zero. Thus, it appears that, the closer to the critical layer, the more important is the absorption due to nonlinearity and turbulence in comparison with absorption into the mean flow. On the other hand, even without turbulence absorption, the energy flux also vanishes at the critical layer irrespective of R_c (see (15) and (16)).

3 Reflection of incident wave

By matching the boundary conditions at x_m we can find the reflection coefficients of the gravity waves in the context of a multi-layer model. The numerical solutions within any layer centered about $\underline{z}$ can be approximated by an upgoing and down going instantaneous plane waves at any position $\underline{z}$

$$\Psi(z) = A(\underline{z})e^{ik_z(z-\underline{z})} + B(\underline{z})e^{-ik_z(z-\underline{z})} \tag{23}$$

where the k_z is the instantaneous vertical wave vector (or the vertical wave vector in the thin isothermal layer within the multi-layer model). The reflection coefficient R at arbitrary position $\underline{z}$ is given by

$$R(\underline{z}) = \frac{|B(\underline{z})|}{|A(\underline{z})|} \tag{24}$$

By taking derivative of (23) with respect to z, we get

$$\Psi'(z) = ik_z A(\underline{z})e^{ik_z(z-\underline{z})} - ik_z B(\underline{z})e^{-ik_z(z-\underline{z})} \tag{25}$$

Combining (23) an (25) we obtain

$$R(\underline{z}) = \left|\frac{ik_z\Psi - \Psi'}{ik_z\Psi - \Psi'}\right|$$

Fig. 2.1, 2.2 and 2.3 show respectively the projected background wind profiles along the zonal, **45°** to the zonal and **315°** to zonal directions. The normalized pressure wave amplitude, Ψ, the location of the

critical level (x=0), the range of the optical potential $(0 < x < x_m)$ where the absorption due to nonlinearity and gravity wave instability occurs, and the range $(x_m < x < x_0)$ where the gravity wave reflection comes primarily from the wind gradient, are all indicated in the Fig. 2.(1-3). In this paper we shall only consider a gravity wave with a period of half an hour and propagating in the three directions. Fig. 2.7, 2.8 and 2.9 show the reflection coefficients of gravity waves versus horizontal phase velocity for different R_c (the "reflection" coefficient at the critical level). From those figgures we can see that with the introduction of even modest absorption the curves are almost identical, which means that the physical processes for reflection at the critical level begin to lose their effectiveness. A further increase in wave absorption to $W_0 = -0.6\lambda$ produces a total reflection coefficient entirely independent of the physics at the critical level x-0, i.e., the same total reflection holds for any value of R_c both in amplitude and phase. Fig. 2.10, 2.11 and 2.12 indicate that when we increase the optical potential the reflection coefficients increase accordingly. The total reflection coefficient ranges from 5% to 25%. The minima (resonance states) occur when the reflected gravity waves from critical level region and background interfere destructively. For isothermal background with constant background wind gradient, the phase of gravity waves near critical level is logarithmically dependent on x, the normalized distance from the critical level. The distance x_0 for a gravity wave with horizontal phase velocity v_h is proportional to v_h. Thus, the phase $\phi \propto \log(v_h)$. For every 2π change in phase we will get a minimum (or maximum). Thus, we have

$$\mu \log \frac{v_{h2}}{v_{h1}} = 2\pi$$

or

$$\frac{v_{h2}}{v_{h1}}=\text{constant}$$

So, for isothermal case, the minima occur more often for small scale gravity waves than for large scale gravity waves. Since this paper is interested in the real atmosphere, we can not get the simple analytic relation between horizontal phase velocity and minima. We can provide qualitative explanations. The instantaneous wave vector k_z can be approximately written as

$$k_z \propto \sqrt{\frac{\omega_b^2-\Omega^2}{\Omega^2}k_x^2-\frac{\omega_\alpha^2-\Omega^2}{c^2}}$$

In the vicinity of the critical level, Ω is small, so the dominant term is $\frac{\omega_b}{\Omega}k_x$. Obviously larger ω_b produces larger k_z and short instantaneous wavelength and therefore more phase change. We would expect more resonance states for larger ω_b. Fig. 2 shows the ω_b profile. We can see from it that ω_b has a peak at about 85km. The critical levels of many gravity waves of interest occur around the peak. those are the gravity waves most affected by the peak, and can be seen from the reflection coefficient profiles. Without this peak we would expect the distance between neighoring minima to increase as horizontal phase velocity increases. As the peak will shorten the distance of neighboring minima, the two competing factors produce more or less evenly separated minima of the reflection coefficient of gravity waves.

Fig. 2.4, 2.5 and 2.6 show what would happen when we vary the wind gradient. It should be pointed out that for realistic wind-profile

gradients, λ is about 40. For $\lambda \approx 1/4$ the wind profile is unrealistically steep. when the background is unstable, i.e., $\lambda \approx 1/4$, the total reflection coefficient can be greater than one, and over-reflection occurs. The over-reflection is a well-known phenomenon[4]. The fact that our optical model correctly predicts the over-reflection for unstable background winds and further more brings both the stable and unstable treatment into a single mathematical framework reinforces the justification of our use of the optical model.

4 Discussion and Conclusion

In this paper we began by investigating the limits of the total reflection from the critical-layer for studying the scattering of incident waves which suffer a loss of energy from numerous diverse and unstructured sources. By setting up a Sturm-liouvile equation, we are able to include in our study the conservation of the time-average energy flux divided by the difference of horizontal phase velocity and the background wind velocity. In this way, we have essentially included the Eliassen and Palm theorems in our formalism.

In this formalism the optical potential takes care of losses other than the loss into the mean flow. The results given in (21) and (22) for the ratio of energy flux without dissipation to the flux with dissipation show that the energy loss through absorption into the mean flow becomes less and less important as compared with losses through instability and turbulence as the gravity wave approaches the critical level. Our particular method also allows us to generalize the result for vertical pressure energy flux to include the absorptive losses ((15(and (16)).

The total downward reflection of a gravity wave from the critical layer region depends on the horizontal phase velocity v_h of the gravity wave, the vertical wind gradient as well as background atmosphere. For stable background winds $(\lambda > 1/4)$ and realistic losses $(|W_0| = 0.45\lambda \approx 0.65\lambda)$ and for realistic wind gradients, the downward reflection coefficient ranges from 5% to 25% which is not sufficient for gravity-wave ducting.

We have also found that for realistic losses in the range $|W_0| = 0.45\lambda - 0.65\lambda$ and for stable background winds, the downward reflection is independent of the physics in the neighborhood of the critical level. The very large viscosity and heat conduction losses expected near the critical level in fact do not play any role; the incident upgoing wave being so reduced in amplitude at such close proximity to the critical level that the reflected wave that closes to the critical layer is negligible, even if the total reflection from the entire critical-layer region (as opposed to the critical level) can be quite significant.

The total reflection coefficient drops down to very low values periodically as a result of resonance absorptions. The resonance absorptions depends, of course, on the background winds and horizontal phase velocity of the gravity wave as expected. The background atmosphere also plays a significant role in determining where the resonance absorptions occur.

For unstable background winds, our optical model shows that over-reflection could occur, in agreement with [4]. The unstable background situation ($\lambda < 1/4$) has been shown to be equivalent to stable background situation ($\lambda > 1/4$) with a source for producing waves instead of a sink for absorbing waves. In this way our method can bring the physics of stable and unstable background winds to within the same framework.

Our original reason for making this investigation is through our awareness of the very short vertical distance over which the incident gravity wave is absorbed compared to its much longer incident vertical

wavelength. This suddenness in the absorption would suggest a breakdown of the WKB approximation resulting in a considerably greater reflection than is generally thought. We were particularly surprised to find that the absorbing negative optical "potential" for a stable background becomes in effect an emitting positive "potential" with an unstable background, thus, bringing both phenomena to within a simple mathematical framework.

In a final comment, recent observations [20] of middle-atmospheric airglow fluctuations using the blocking diagram method of [21] seem to show beyond reasonable doubt the effects of critical-layer blocking on the direction of gravity-wave propagation.

Part III - Perturbation Treatment of minor species' response to gravity waves

1. Introduction

The study of gravity waves in the middle and upper atmosphere has relied from its beginning upon the detection of the motion of minor atmospheric constituents. Early examples include deformations of meteor trails and radio echoes fro mionospheric layers, while more recently many observations have been made of airglow intensity fluctuations and resonance lidar backscatter fluctuations.

Many of the minor constituents of the atmosphere are distributed in layers which are sharply peaked. The atomic sodium layer, for example, is concentrated around 90 km in a layer which has on average a half-width much less than the atmospheric scale height. Because of such background structures, small-amplitude gravity waves can induce local fluctuations of much larger amplitude in minor species concentration. Modeling the response of minor atmospheric species to gravity wave perturbations has been carried out by many investigators(Thome [39]; Porter et al. [36]; Chiu and Ching [25]; Weinstock [42]; Hatfield et al.[27]; Molina [34]; Gardner and Shelton [26]; Walterscheid, et al. [41]; Hines and Tarasick [41]; Hickey [28]. With the exception of weinstock [42] and Gardner and Shelton [26]), previous studies have focused on the linear response. The present work develops a perturbation expansion approach that can be used to model the nonlinear response of neutral minor species to linear gravity waves. The method has obvious application to charged layers to the extent

that neutral dynamics determine the charged species motion. The approach taken is Eulerian, so that the method has direct application to measurements made at a fixed height. It is apparent that, with the inherent reliance of many technologies (ionosondes, airglow photometers, radars, lidars) on the detection of minor species motions, a clear understanding of the response of neutral minor species layers to linear gravity waves is essential for the proper interpretation of such data, particularly when the data are spectrally analyzed.

Section 2 discusses the origin of the nonlinear dynamical response of minor species with sharply peaked profiles. Section 3 develops the perturbation expansion method in general, and in section 4 it is used to calculate higher-order terms in the minor species dynamical response over a broad range of wave parameters as well as for illustrative specific cases. Conclusions are presented in section 5.

2. Dynamical Nonlinearity

2.1 . Minor species velocity, diffusion, and chemistry

Linear gravity wave theory has on the whole been developed for the special case of a homogeneous fluid, where the mean molecular mass is constant and mixing processes overwhelm diffusive separation. This is in general a good approximation below the turbopause. However, near and above 100 km, the mean molecular mass becomes strongly variable with increasing altitude, and at the same time the mean free path is large enough for species to separate diffusively. In the thermosphere, therefore, even for the neutral minor species, a proper treatment of the response to gravity wave perturbations must incorporate multi-component fluid effects and have separate momentum equations for each component (Mayr and Volland [33]). In the present paper, attention is restricted to neutral minor species in the stratosphere and mesosphere. In these regions, where minor species concentrations never exceed 1% of the total atmospheric concentration, one is justified in considering only the continuity equation for the investigation of neutral minor species. This is because the overwhelming majority of minor species collisions are with major-species particles, and one can assume that they have the same velocity as the major species, which velocity we denote by $\bar{v}$, except possibly for diffusion, which we consider next.

The Eulerian continuity equation for any minor species is

$$\frac{\partial n}{\partial t} = -\nabla \cdot \left(n \bar{v}_m \right) + P - nL \qquad (1)$$

where $n(x,y,z,t)$ is the minor species number density, $\vec{v}_m(x,y,z,t)$ is the minor species velocity field, P is the minor species production rate per unit volume, and L is the minor species loss frequency. Since we want our theory to apply to airglow emission as well as active probing, we will take the term minor species, in such cases, to mean the particular electronic or vibrational state of the species which is the source of the airglow. We wish to use this equation to examine the response of a minor species to dynamical perturbations induced by a gravity wave, in particular the nonlinear response to such perturbations.

Other processes which must be considered, in addition to wave-induced dynamical perturbations, are diffusive processes and "chemical" (including collisional and radiative) production and loss. Even in the absence of any motion of the atmosphere as a whole, it may be that $\vec{v}_m \neq 0$. This is because any minor species with a layered structure is in diffusive, not hydrostatic, equilibrium, and is therefore continually diffusing from regions of net production to regions of net loss. The steady-state vertical diffusive velocity for an isothermal atmosphere is given by (Chamberlain and Hunten, [24])

$$w_{diff} = -D\left(\frac{1}{n_o}\frac{dn_o}{dz} + \frac{m_n g}{kT}\right) \qquad (2)$$

where D is the diffusion coefficient, m_n the molecular mass of the minor species, g is the acceleration due to gravity, k is Boltzmann's constant, and T is the temperature. For pure gravity wave motion with parcel velocity $\vec{v}$,

so long as $|\bar{v}| >> |w_{diff}|$, the effects of steady-state diffusion will be negligible in equation (1). However, for sufficiently small-scale waves it may be that $|\bar{v}| \approx |w_{diff}|$, and even for somewhat larger-scale waves the diffusive velocity may be comparable to the gravity wave velocity for an appreciable part of each gravity wave period, as $\bar{v}$ passes through zero twice per cycle.

In addition to steady-state diffusion, the effects of chemistry must be considered in treating equation (1). It may be that perturbations to the chemical production and loss terms induced by the gravity wave motion are comparable to the other perturbation terms. If this were the case, the effects of chemistry could easily be as important as dynamical effects in determining minor species density fluctuations.

One straightforward measure of the importance of the effects of diffusion and/or chemistry versus dynamical effects can be made by noting whether the diffusion time τ_{diff}, or chemical lifetime τ_{chem}, is less than, or of the order of, the wave period T (Walterscheid et al. [41]). The range of diffusion times and lifetimes of minor constituents, from seconds to days (Winick [43]), encompasses the gamut of gravity wave periods, which are from 5 or 6 minutes up to several hours. Thus, whether or not steady-state diffusion or perturbations to the production chemistry should be incorporated in the solution to equation (1) must be decided on a case by case basis. For example, for the OH(v') levels, which are the source of the Meinel bands, $\tau_{chem} \approx 10^{-2} - 10^{-3} s$ due to radiation alone and shorter with quenching, so "chemistry" must be included. Similarly, the $O_2(b^1\Sigma_g)$ state, which is the source of the O_2 atmospheric bands, is short-lived, with a radiative lifetime of 12 s, and perturbations of chemistry by the wave must

be considered. For total atomic sodium density in the lower thermosphere, on the other hand, the effective chemical lifetime is longer than 5 minutes, except on the bottomside of the *Na* profile near 85 km, and diffusion times are much longer than typical gravity wave periods (Swider [38]). Thus chemistry and diffusion may be safely neglected in calculating wave-induced perturbations of atomic sodium.

Since the focus of this paper is on gravity wave related dynamics, we will neglect steady-state diffusion as well as perturbations to the chemistry and consider only the wave-induced velocity. Under these assumptions, equation (1) becomes

$$\frac{\partial n}{\partial t} = -\nabla \cdot (n\vec{v}_m). \tag{3}$$

Here, we cannot in general assume that $\vec{v}_m$ equals the gravity wave velocity as is usually done because we also include in our investigations the higher-order nonlinear response terms. we will show in detail in section 3 how these higher-order terms induce a minor species drift velocity which vanishes only if the gravity wave is stationary along the vertical directions. This drift velocity, which is in addition to any steady-state diffusive velocity, is determined through a term-by-term removal of secular terms which arise in the perturbation expansion. Thus, $\vec{v}$ becomes an algebraic sum of the gravity wave velocity and the higher-order wave-induced drift velocities and we may write

$$\vec{v}_m = \vec{v} + w_d \hat{k}, \tag{4}$$

where $\bar{v}$ is the gravity wave velocity, w_d is the gravity wave induced drift velocity, and $\hat{k}$ is the unit vector in the vertical direction. Since $\bar{v}$ is known, equation (3) is an uncoupled equation for n only.

2.2 Minor species density

We will now briefly outline the origin of the nonlinear minor species density response, first pointed out by Weinstock [42]. To simplify the analysis, for the remainder of this paper we shall assume that the gravity wave is monochromatic, linear gravity wave with angular frequency ω, horizontal wavenumber k_x, vertical wavenumber k_z, propagating in a windless, isothermal, horizontally stratified atmosphere with velocity components u and w in suitably chosen Cartesian coordinates such that

$$\bar{v} = (u, 0, w)$$

and with x and t dependence given by exp $i(\omega t - k_x x)$. Such a wave is a solution to the linearized hydrodynamic equations of the major atmospheric species, implying that the major species number density (hereafter denoted by N) is fluctuating with a small amplitude about an unperturbed, background value. Given this, we can write the relative fluctuation in the major species number density directly from the linearized continuity equation as

$$\frac{N'}{No} = \frac{k_x}{\omega} + \frac{i}{\omega}\frac{\partial w}{\partial z} + \frac{i}{\omega}\frac{1}{No}\frac{dN_o}{dz}w \qquad (5)$$

where $N'(x,z,t)$perturbed part of N and $No(z)$=unperturbed part of N. The linear gravity wave described above will induce a fluctuation in the minor species density. However, it is important to note that the minor species fluctuation is not necessarily a "wave" in the same sense as the major species fluctuation is a wave. While the latter is a solution to the entire set of linearized, coupled hydrodynamic equations for a fluid, the former is the response of a minor constituent embedded in the fluid to wave-induced perturbations and is the solution to just the uncoupled continuity equation given by (3) for the minor species number density n. this is true because of the neutral minor species in the stratosphere and mesosphere which we are considering the momentum equation is overwhelmingly dominated by the collision term representing momentum transfer from particles of the major species. For the present, as we are addressing the first-order response, we will take $\bar{v}_m = \bar{v}$, and linearizing (3) in a fashion analogous to the derivation of equation (5) for the major species, obtain the first-order approximation to the minor species response

$$\frac{n'}{n_o} = \frac{k_x}{\omega} + \frac{i}{\omega}\frac{\partial w}{\partial z} + \frac{i}{\omega}\frac{1}{n_o}\frac{dn_o}{dz}w \qquad (6)$$

where $n'(x,z,t)$perturbed part of n and $n_o(z)$=unperturbed part of n.

Two points to consider about the minor species response, evident in the first-order equation (6), are the following. First, for minor species with a layered structure, the unperturbed density gradient is positive in the region below the peak and negative in the region above the peak, while the unperturbed major species gradient is always negative. This implies a 180°

shift in the phase difference between the major and minor species density fluctuations at the point of the minor species peak. This phase reversal in the region of the profile peak has been known for some time on both theoretical (Thome [39]; Porter et al.[36]; Weinstock [42]) and observational grounds (Thome [39]; Noxon [35]; Shelton et al [37]).

A second point to consider regarding equation (6) is its magnitude relative to equation (5). For the case of pure linear gravity wave motion which we are considering, the magnitude of the major species fluctuation, given by (5), is by assumption small, say 10% or less. However, when the same velocity field is used in (6), the magnitude of the first-order minor species response can be much greater, because the adjective part of the Eulerian time derivative, which produces the third terms of (5) and (6), involves gradients of background densities. As mentioned, such gradients can be much larger for minor species than the corresponding major species gradient. Consequently, through (5) is by assumption valid for the major species, retaining only first-order terms for the minor species, as in (6), is not in general justified. As an explicit example, if one uses the U.S Standard Atmosphere (USSA) 1976 model of atomic oxygen, at 90 km (below the O peak at 97 km) a gravity wave which corresponds to a 10% density fluctuation in the major species will induce a 40% first-order fluctuation in the atomic oxygen density. Thus dynamical nonlinearities enter naturally into the minor species response. In the next section, a method is developed to treat these dynamical nonlinearities.

3. Perturbation Expansion Method

To calculate the higher-order solutions to equation (3), we assume for the moment $\bar{v}_m = \bar{v}$, and we rewrite (3) in terms of $\bar{v}$ as (Isler et al [30])

$$\frac{\partial \psi}{\partial t} = -u\frac{\partial \psi}{\partial x} - w\frac{\partial \psi}{\partial z} - S\psi - S \tag{7}$$

where

$$\psi \equiv n'/n_o$$

$$S = -\left(\frac{\partial u}{\partial x} + \frac{\partial w}{\partial z} + \frac{1}{n_o}\frac{dn_o}{dz}w\right)$$

Note that now n' means all the perturbation terms, not just the first order. Since S is given, equation (7) is a homogeneous equation and can be readily solved. We write

$$\psi = \lambda\psi_1 + \lambda^2\psi_2 + \lambda^3\psi_3 + \ldots \tag{8}$$

and set $\bar{v} \to \lambda\bar{v}$, where λ is a dimensionless parameter introduced as a bookkeeping device to keep track of orders in $\bar{v}$ for ψ_n, with n=1,2,3,...., or equivalently of orders in N'/N_o, since u and w are linearly related to N'/N_o, Thus, ψ_1 depends linearly on $\bar{v}$, ψ_2 has a quadratic dependence, etc.. Inserting (8) into (7) and equating the coefficients of λ^n for each n, we obtain an infinite set of recursion relations, one for each value of n.

It may be suggested that to be consistent, one would have to retain all nth order terms, and so in (7) put in for $\bar{v}$ the expansion

$$\bar{v} = \lambda\bar{v}_1 + \lambda^2\bar{v}_2 + \lambda^3\bar{v}_3 + \ldots$$

These higher orders in $\bar{v}$would be the result of retaining higher orders the coupled hydrodynamic equations of the major species, i.e. incorporating the effects of a nonlinear gravity wave. However, we have assumed that the minor species fluctuations are due to linear gravity wave, that is $\bar{v} = \bar{v}_1$ to a good approximation, so we further assume that any contributions to the minor species response due to higher-order corrections to $\bar{v}$ are negligible relative to those due to the linear $\bar{v}$ alone. This was also implicitly assumed by Weinstock and Gardner and Shelton (1985).

To the first order in λ, setting $\bar{v} = \lambda\bar{v}$ and taking equation (8) into account, eqaution (7) reads

$$\frac{\partial \psi_1}{\partial t} = S$$

and so we can write

$$\psi_1 = -\int_{t_o}^{t}\left(\frac{\partial u}{\partial x} + \frac{\partial w}{\partial z} + \frac{1}{n_o}\frac{dn_o}{dz}w\right)dt'. \qquad (9)$$

Since we are interested in fluctuations at some time t lone after the gravity wave has settled into its monochromatic state, we take the initial time in (9), $t = t_o$, to be a time before gravity wave motion begins, when $\bar{v}$=0. We assume that the transient state develops smoothly and continuously

into a monochromatic state. as it should be, ψ_1 obtained in this way is equivalent to equation (6). Using the above notation, $\psi_1 = \mathrm{Re}\{-iS/\omega\}$.

When calculating higher-order solution to equation (7), it must be remembered that the real parts of complex quantities must be taken prior to any multiplication; otherwise, difference-frequency effects can be missed altogether (in particular, the dc contribution to the second-order response will be missed, as will the component of the third-order response at the fundamental frequency). thus, to second order in λ, equation (7) is given by

$$\mathrm{Re}\frac{\partial \psi_2}{\partial t} = -\mathrm{Re}u\,\mathrm{Re}\frac{\partial \psi_2}{\partial x} - \mathrm{Re}w\,\mathrm{Re}\frac{\partial \psi_1}{\partial z} - \mathrm{Re}S\,\mathrm{Re}\psi_1 \qquad (10)$$

Equation (10) can be solved since ψ_1 is known from (9). Once again, the integration is chosen to be from a time prior to the arrival of the gravity wave. When treating the case of a gravity wave which is traveling along the vertical (it is always a traveling wave along the horizontal), the three nonlinear terms on the right-hand side of (10) contain a constant time-independent term. Such a term is analogous to similar constant terms, called secular terms, that occur in higher than first-order perturbation treatment of simple one-dimensional nonlinear systems. in this paper through a renormalization of some of the parameters in the system; in this paper we have used the Krylov-Bogoliubov-Mitropolsky renormalization method. the renormalized parameters are shifted by a constant value as a result of the nonlinearity. In our case, we renormalize the vertical component of the minor species velocity by introducing w_d whose

introduction is to cancel the secular terms. This drift velocity is not to be confused with the Stokes' drift, since the latter arises as a result of nonlinearity in the hydrodynamic equations for the major species, while in our present case the drift velocity is a drift of the minor species induced by a vertically traveling linear gravity wave; in both cases, however, the drift velocity vanishes for a vertically stationary wave.

With $\vec{v}_m = \vec{v} + w_d\hat{k}$, equation (7) is now

$$\frac{\partial\psi}{\partial t} = -u\frac{\partial\psi}{\partial t} - w\frac{\partial\psi}{\partial z} - S\psi - S - \frac{1}{n_o}\frac{\partial(n_o w_d)}{\partial z} \qquad (11)$$

As before, we write

$$\psi = \lambda\psi_1 + \lambda^2\psi_2 + \lambda^3\psi_3 + \cdots$$

but in addition we now write w_d as

$$w_d = \lambda w_{d1} + \lambda^2 w_{d2} + \lambda^3 w_{d3} + \cdots$$

Everything proceeds as before, equating the coefficients of λ^n to obtain the nth-order solution to (3). In particular, the second-order equation (10) becomes

$$\frac{\partial\psi_2}{\partial t} = -\mathrm{Re}u\,\mathrm{Re}\frac{\partial\psi_1}{\partial x} - \mathrm{Re}w\,\mathrm{Re}\frac{\partial\psi_1}{\partial z} - \mathrm{Re}S\,\mathrm{Re}\psi_1 - \mathrm{Re}\frac{1}{n_o}\frac{\partial(n_o w_{d2})}{\partial z} \qquad (12)$$

while in general, the nth-order recursion relation takes the form

$$\frac{\partial \psi_n}{\partial t} = \mathrm{Re}\, u\, \mathrm{Re}\frac{\partial \psi_{n-1}}{\partial x} + \mathrm{Re}\, w\, \mathrm{Re}\frac{\partial \psi_{n-1}}{\partial z} + \mathrm{Re}\, S\, \mathrm{Re}\, \psi_{n-1} - \mathrm{Re}\frac{1}{n_o}\frac{\partial (n_o w_{dn})}{\partial z} \qquad (13)$$

In this way, with the appropriate renormalization, one can obtain ψ, the minor species nonlinear response, to any order in the gravity wave velocity.

For the gravity wave velocity, we use a generalization of the Hine's linear gravity wave theory (Hines [44]) which allows for partially ducted waves, so that we write for $\vec{v}$,

$$u = \bar{u}(z) e^{i(wt - k_x x)} \left[e^{i(k_z z + \pi - \phi)} + \mathrm{Re}^{-i(k_z z - \phi)} \right] \qquad (14)$$

$$w = \bar{w}(z) e^{i(wt - k_x x)} \left[e^{ik_z z} + \mathrm{Re}^{-ik_z z} \right] \qquad (15)$$

where

$$\phi = \tan^{-1} \eta / k_z$$

$$\eta = -(1 - \gamma/2) g / c^2$$

$$\bar{u} = A w k_x c^2 \left[k_z^2 + \eta^2 \right]^{1/2} e^{z/2H}$$

$$\bar{w} = A w \left[w^2 - k_x^2 c^2 \right] e^{z/2H}$$

R=complex reflection coefficient

A=wave amplitude

In (14) and (15), R is the reflection from higher altitudes, and $\bar{u}$ and $\bar{w}$ are both real.

Substituting (14) and (15) into (12) we find we can remove the secularity if

$$\frac{1}{n_o}\frac{\partial(n_o w_{d2})}{\partial z} = \left(1-|R|^2\right)\frac{\bar{w}}{2\omega}\left(\bar{u}k_x\cos\phi + \bar{w}k_z\right)\left[\frac{1}{n_o}\frac{\partial(n_o)}{\partial z} - \frac{1}{H}\right] \qquad (16)$$

Clearly, for a vertically stationary wave, since $|R|=1$, the secularity vanishes and there is no induced vertical drift velocity.

We can rewrite (16) as

$$\frac{1}{n_o}\frac{\partial(n_o w_{d2})}{\partial z} = \left(1-|R|^2\right)\left(k_x\cos\phi D_1 + k_z D_2\right)\left[\frac{1}{n_o}\frac{\partial(n_o)}{\partial z} - \frac{1}{H}\right] \qquad (17)$$

where

$$D_1 = \bar{u}\bar{w}/2\omega$$
$$D_2 = \bar{w}^2/2\omega$$

Comparing (17) with (2), we see that D_1 and D_2 have the units of a diffusion coefficient, and so behave as wave-induced diffusion coefficients, since they depend quadratically on the amplitude of the gravity wave velocity and would both vanish as $\bar{v}\to 0$. Also, not unexpectedly, both

would increase with longer period waves. The analogy should not be drawn too far, though, since the H used here is the major species scale height.

Given the important role gravity waves play in the motion of the middle atmosphere, we believe this wave-induced diffusion could have significant effects in determining minor species distributions. It is important to remember that the wave-induced diffusion considered here is distinct from any diffusion due to a gravity wave field which is nonlinear, such as eddy diffusion. The wave-induced diffusion we consider is due solely to a linear gravity wave, and acts selectively on a particular minor species.

For the remainder of this paper, we shall consider only two gravity wave models: a freely traveling wave model (Hines [44]) and a vertically stationary model which satisfies a rigid surface ground boundary condition. This means we will consider only the cases for $|R|=0$ and $|R|=1$.

Gardner and Shelton [26] devised a similar perturbation expansion approach; they too neglected production and loss perturbations, and began, as we have done, from equation (3). However, their approach assumed a form for the solution in advance, and they considered only large period gravity waves, while the approach taken here is more general. In addition, their formalism also leads to a secularity problem, which they did not address.

For the remainder of this paper, we shall consider only two gravity wave models: a freely traveling wave model (Hines [44]) and a vertically

stationary model which satisfies a rigid surface ground boundary condition. This means we will consider only the cases for $|R|=0$ and $|R|=1$.

4. Numerical Results

We have calculated the minor species response to third order in the linear gravity wave for several different background profiles and over a wide range of gravity wave parameters. As one would expect, the importance of the higher-order terms in the response depends strongly upon the steepness of the vertical density gradient of the minor species. In developing the model, we used Chapman functions and Gaussian distributions for analytic models of minor species profiles, as well as the USSA 1976 model of atomic oxygen. We also investigated the effects of varying the horizontal phase speed of the perturbing gravity wave at a fixed period and found that the importance of the nonlinear terms was overall not sensitive to such variations. for purposes of illustration in this paper, we show results employing a Chapman-like layer as the minor species model profile. The layer is specified with a full-width at half-maximum of $\approx 5\ km$ and an implied scale height, given by $\left[\frac{1}{n_o}\left|\frac{dn_o}{dz}\right|\right]^{-1}$, of $\approx 2\ km$ on the bottomside of the layer; the layer peak is taken to be at 90 *km* (Figure 1). This can be thought of as a generic minor species profile, which under suitable atmospheric conditions could represent the profile of the OH Meinel emission, the atomic sodium layer, the D region electron layer, or other layered distributions. Again we emphasize that the focus here is solely on the effects of dynamical perturbations to the layer, recognizing that in many cases of interest this will give an incomplete picture of the actual fluctuations of species concentration, which can also be strongly affected by photochemistry and radiative processes. To illustrate the importance of nonlinear effects over a range of wave parameters, we

chose three representative gravity waves: one of small scale, one of medium scale, and one of large scale.

We normalize the envelope of the amplitude of the velocity field to induce at most a 5% major species density fluctuation at he peak of the minor species profile. This is done to ensure that the gravity wave field itself is, to a good approximation, linear. Using this normalization, it can be shown that the wave field is convectively stable for all wave parameters and heights considered, further supporting the assumption of linearity. In figure 3.(2-6), the minor species density response has been plotted over two wave cycles at each of three altitudes: one below the peak, one at the peak, and one above the peak.

As a typical medium-scale gravity wave of the mesopause region, we first consider a freely traveling wave ($|R|=0$) with horizontal phase trace speed $v_{phx}=75m/s$ and intrinsic period $\tau=1hr$; the horizontal and vertical wavelengths of this wave are 270 *km* and 23 *km*, respectively. The results for this particular gravity wave are not unusual, and we have used it solely for illustrative purposes. In Figure 3.2, we have plotted the first, second, and third-order minor species response. Figure 3.3 shows the sum of the first three orders in the minor species response (dashed), compared to the first-order response alone (solid) and the major species density fluctuation of the linear wave field (dotted).

The lower panels of Figure 3.2 and 3.3 show the response at 87 *km*, where the background minor species density is $\approx 15\%$ of its peak value. the first-order minor species response here is greater than 18 times the major

species relative fluctuation, and consequently the nonlinear response at this height is considerable. The second-order response, roughly in phase with the first-order response for half the wave period at this altitude, gives rise to a cusping effect, resulting in a sharpening of the waveform peak and a flattening of the trough, seen clearly in the lower panel of Figure 3.3. In this case, the nonlinear response seems to converge rapidly and the response up to third order is expected to represent the infinite-order response rather well.

The middle panels of Figure 3.2 and 3.3 show the response at 90 km, the profile peak. Here, though the vertical density gradient passes through zero, the second derivative of the density profile reaches a maximum. As a results, the nonlinear response at this height remains significant. But here, the second-order response is out of phase with the first order response near the first-order peaks, and so the cusping effect is reversed, with the crests being flattened rather than the troughs. the upper panels of Figures 3.2 and 3.3 show the response at 93 km, above the layer peak. Here the minor species scale height is larger than below the peak, and the response is for the most part linear. Notice the phase shift of the minor species density response relative to the major species at the profile peak. For waves with large λ_z, as in Figure 4 below, this phase shift approaches 180 degrees.

In Figure 3.4, results similar to Figure 3.3 are plotted for a wave which is stationary in the vertical ($|R|=1$). This large-scale wave has $v_{vphx}=250 m/s$ and a period of 2 hr, with a horizontal wavelength of 1800 km and a vertical wavelength of 369 km. This phase speed is roughly that of the principal thermospheric guided mode, ducted by the sharp

temperature rise above the mesopause (Tuan and Tadic [45]), and so is an appropriate choice for which to consider the stationary wave case. For stationary waves, the higher orders are always in phase with the primary wave at the beginning of the primary wave cycle, and the nonlinear cusping effect is thereby reinforced. Evidence of some cusping can be seen at all the heights in Figure 3.4.

Small-scale waves in the mesopause region can be ducted by the background atmospheric structure, for example by background winds (Chimonas and Hines [46]) or by variations in the stable stratification. In Figures 3.5 and 3.6, we show (in the format of Figure 3.3) results for a small-scale wave with $v_{phx} = 35 m/s$, a period of 12 *min*, horizontal wavelength of 25 *km*, and a vertical wavelength of 11 *km*.
Figure 3.5 shows the results for the $|R| = 0$ (traveling wave) case, while Figure 3.6 shows those for the $|R| = 1$ (stationary wave) case. Because of the short vertical wavelength ,the first-order response at 87 *km* in the stationary wave case, though still substantial enough to cause considerable cusping, is much less than in the traveling wave case. This is due to the fact the amplitudes are normalized based on the major species density fluctuation at 90 *km*, which is about a quarter of a vertical wavelength and so 90 degrees out of phase with that at 87 *km*. However, the importance of the nonlinear response at all the heights considered is apparent in either case.

The above results demonstrate the significance of the nonlinear response for minor atmospheric constituents which are distributed in narrow layers. this leads, for example, to a pronounced cusping effect in

the response at certain height levels. As a consequence, it is to be expected that the spectra obtained from minor species fluctuations at particular height levels can contain peaks not only at frequencies associated with actual gravity wave field, but at harmonics of the gravity wave frequencies as well. In fact, there exists in the literature some observational evidence as such harmonics (Shelton et al.[37]).

5. Conclusions

We have outlined a method which can be used to calculate higher-order, nonlinear terms in the local response of minor atmospheric species to linear gravity waves. The method results in an expansion of the minor species response to any order in the linear gravity wave. We have generalized the Krylov-Bogoliubov-Mitropolsky method for removing secularities to the case for field equations, and in the process have discovered a potentially significant diffusion mechanism for minor species with steep concentration gradients. Higher-order effects in the minor species response have been shown to be important over a broad range of wave parameters. Consequently, particular care must be taken in inferring from the power spectra of minor species fluctuations. In future work we intend to extend the method to treat charged minor species and incorporate the effects of perturbations to production and loss processes.

Bibliography

[1] R. S. Lindzen, Q. J. R. Meterol Soc. **93**, 1842, 1967

[2] R. S. Lindzen, Proc. R. Soc London Ser. A303 229-316, 1968A

[3] R. R. Hodges, J. Geophys. Res. **74**, 4087-4090, 1969

[4] R. S. Lindzen and D. Blake, Geophys. Fluid Dyn. **2**, 31-61, 1971

[5] H. Volland, Journal. Geophys. Res. **74** 1786, 1969b.

[6] Francis, S. H. J. Geophy Res **78**, 8289, 1971

[7] C.O. Hines, C. A. Reddy, J. Geophys. Res. **72**, 567(1967).

[8] J. R. Booker, F. P. Bretherton, J. Fluid Mech. **27**. 513 (1967).

[9] P. Hazel, J. Fluid Mech. **30**, 775 (1967).

[10] W. L. Jones, J. Fluid Mech. **34**, (1968).

[11] J. E. Geisler, R. E. Dickinson, J. Atmos. Sci. **31**, 946 (1975).

[12] M. A. Geller, H. Tanaka, D. C. Fritts, J. Atmos. Sci. **32**, 2125, (1975).

[13] D. C. Fritts, M. A. Geller J. Atmos. Sci. **33**, 2276 (1976)

[15] D. C. Fritts, J. Atmos. Sci. **36** 1223 (1979)

[14] H. Fan, Optical model treatment of gravity wave - critical layer interaction (1992)

[16] L. I. Schiff, Quantum mechanics, 3rd edition, McGraw-Hill, (1968).

[17] .A.D. Richmond, J. Geophys. Res. **83**, 4143 (1978).

[18] .NCAR CEDAR Data base Catalogue (1990), National center for Atmospheric Research, Boulder, Colorado.

[19] .J. M. Forbes, D. F. Gillette, Rep. AFGL-TR-82-0173(I), AFGL(now Phillips Lab.) Hanscom AFB(1982).

[20] M. J. Taylor, E. H. Ryan, T. F. Tuan, R. Edwards, J. Geophys. Res. **97**, 2301 (1992).

[21] .M. J. Taylor, E. H. Ryan, T. F. Tuan, Amer. geophys. Union, **72**,

374 (1991).

[22] .W. L. Jones, J. Fluid Mech. **34**, 609, (1968).

[23] D. Y. Wang, T. F. Tuan, J. G. R. **93**, 9916 (1988)

[24] J. W. Chamberlain. and D. M. Hunten. Theory of Planetary Atmospheres, Academic Press. (1987)

[25] Y. T. Chui and B. K. Ching. Geophys. Res. Lett., **5**, 539. (1978)

[26] C. S. Gardner and J. D. Shelton J. Geophys. Res., **90**, 1745 (1985).

[27] R. Hatfield, T. F. Tuan and S. M. Silverman J. Geophys. Res., **86**, 2429 (1981).

[28] H. Hickey J. Geophys. Res., **93**, 4077 (1988).

[29] C. O. Hines and D. W. Tarasick Planet. Space Sci., **35**, 851. (1987).

[30] J. R. Isler, T. F. Tuan, U. Makhlouf, R. H. Picard and P. L. ¹Lin EOS, **69**, 1342 (1988).

[31] J. R. Isler, T. F. Tuan, R. H. Picard and U. Makhlouf J. Geophys. Res., **96**, 14141 (1991).

[32] U. Makhlouf, D. Y. Wang, J. J. Lin and T. F. Tuan EOS, **68**, 44, 1394 (1987).

[33] H. G Mayr and H. Volland J. Geophys. Res., **81**, 671. (1976).

[34] A. Molina J. Atmos. Sci., **40**, 2444 (1983).

[35] J. F. Noxon Geophys. Res. Lett., **5**, 25 (1978).

[36] H. S. Porter, S. M. Silverman and T. F. Tuan J. Geophys. Res., **79**, 3827 (1974).

[37] J. D. Shelton, Gardner, C. S. and C. F. Sechrist Geophys. Res. Lett., **7**, 1069 (1980).

[38] W. Swider Planet. Space Sci., **34**, 603 (1980).

[39] G. Thome J. Geophys. Res., **73**, 6319. (1968).

[40] U.S. Standard Atmosphere U. S. Government Printing Office, Washington, D. C (1976).

[41] R; L Walterscheid., G. Schubert and J. M. Straus J. Geophys. Res., **92**, 1241 (1987).

[42] J. weinstock J. Geophys. Res. **83**, 5175 (1978).

[43] J. R. Winick Solar-Terrestrial Physics, edited by J. M. Forbes and R. L. Carovillano, D. Reidel Publishing Company, Dordrecht, Netherlands (1983)

[44] C. O. Hines Can. J. Phys. 38, 1441, 1960

[45] T. F. Tuan and D. Tadic J. Geophys. Res. 87, 1648, 1982

[46] Chimonas and C. O. Hines J. Geophys. Res. 91 1299, 1986

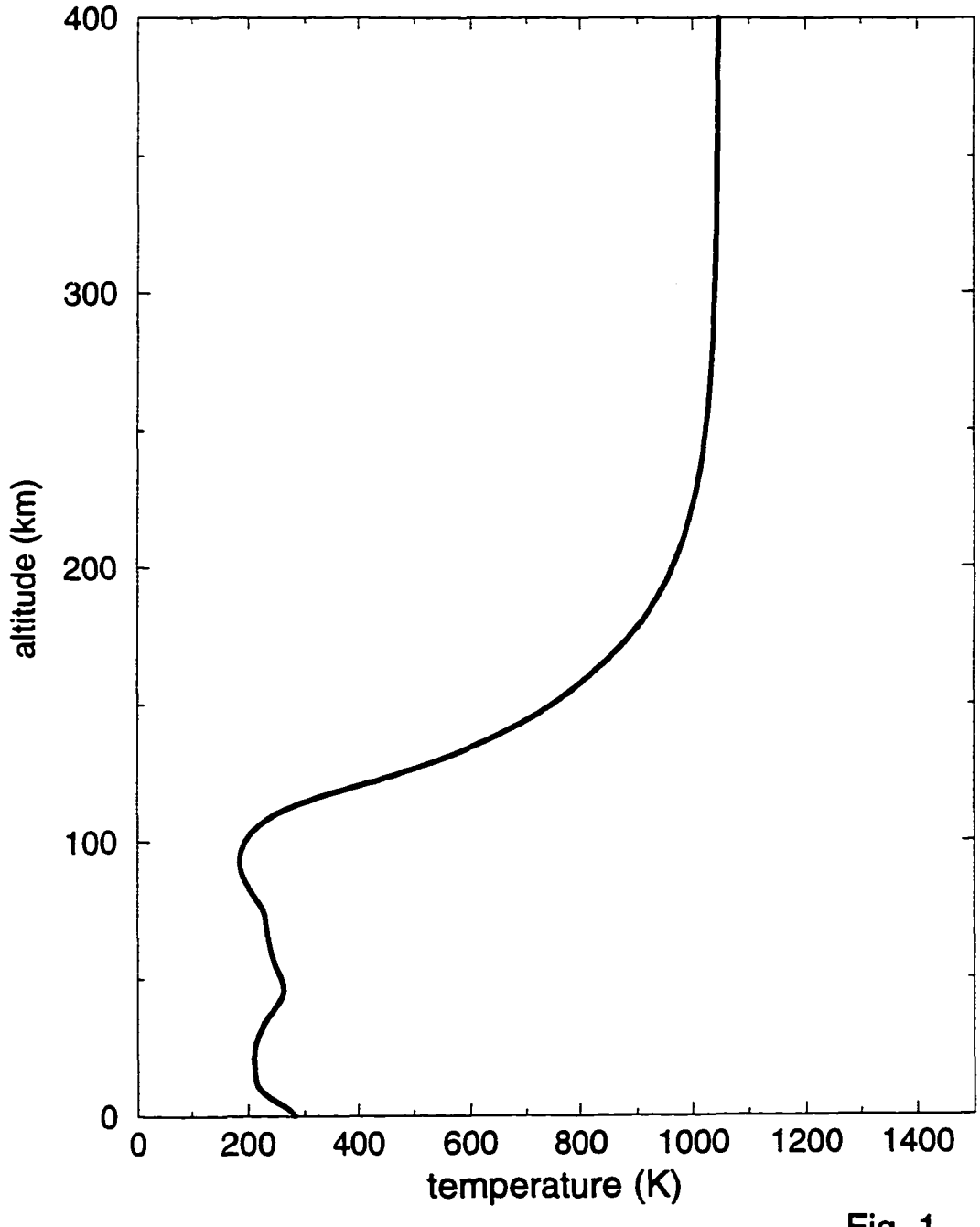

Fig. 1

background Brunt frequency vs height

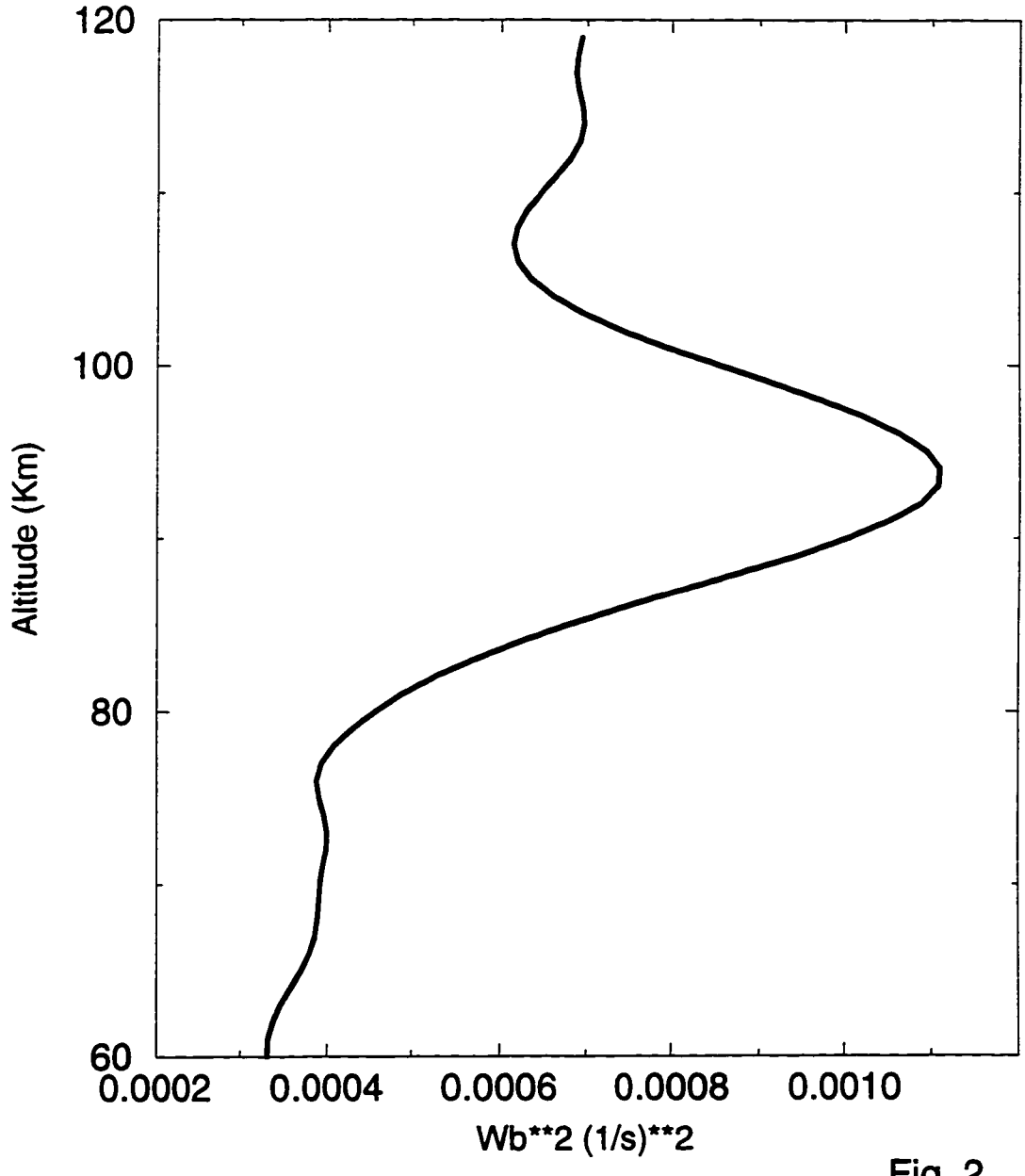

Fig. 2

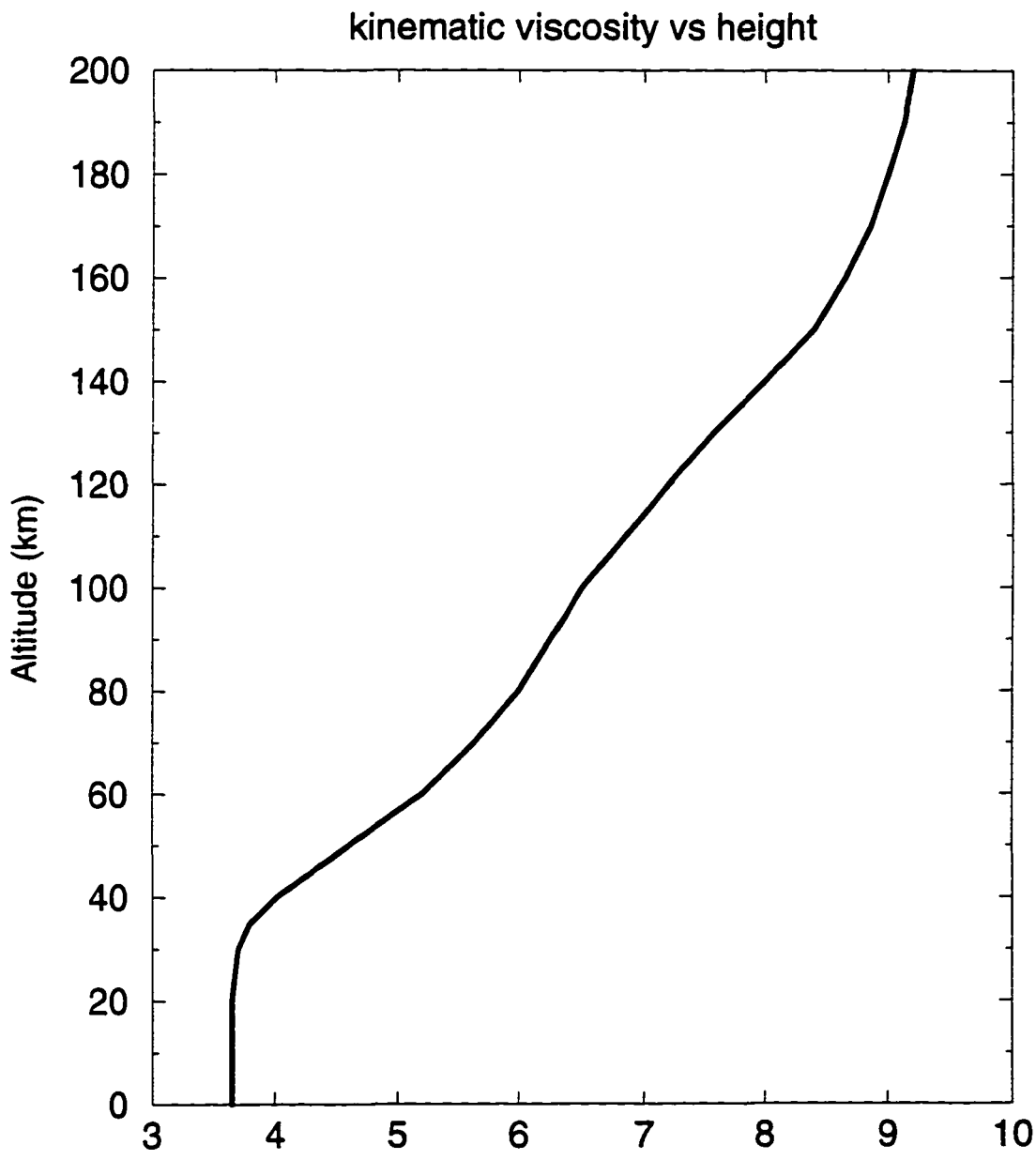

Fig. 3

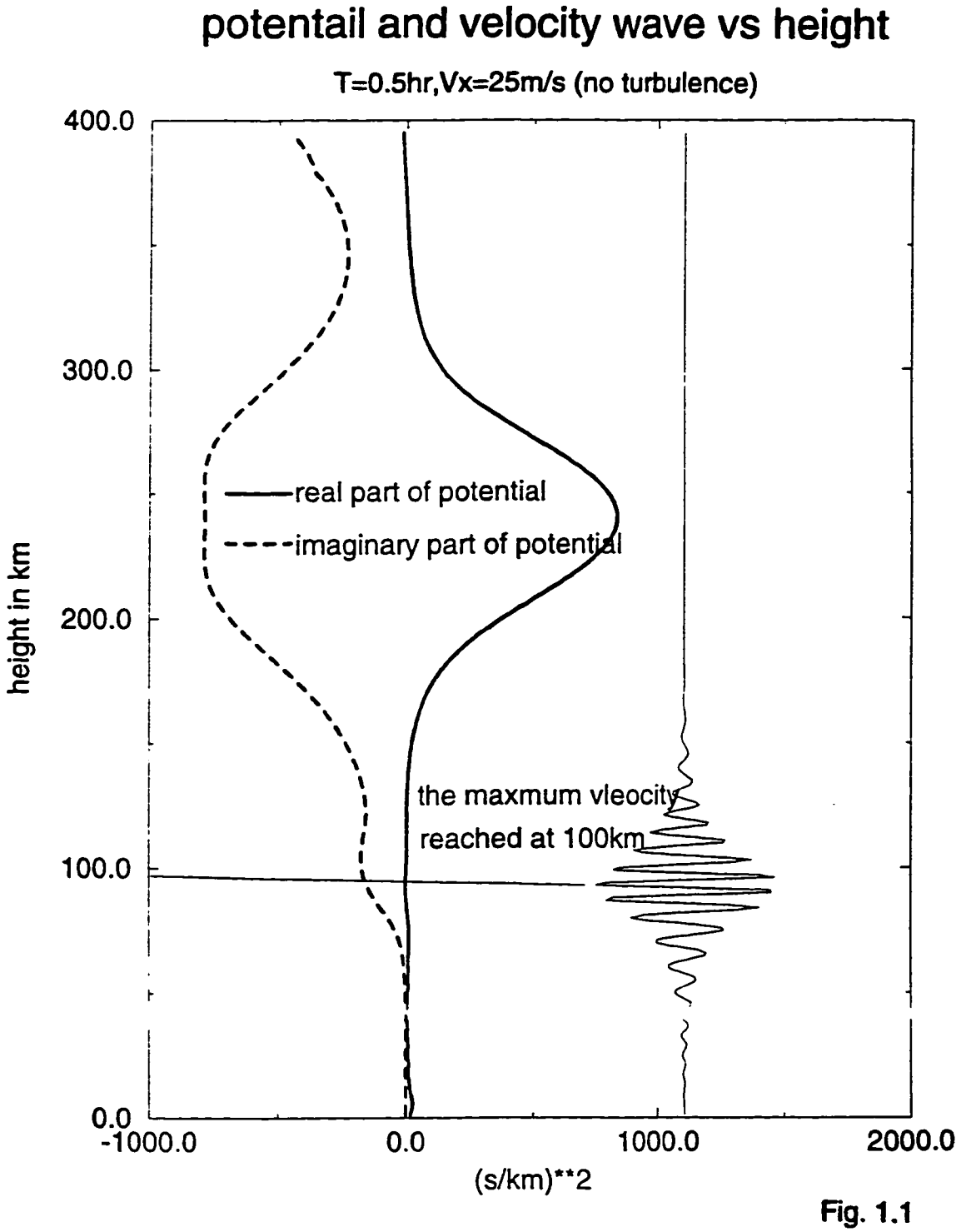

Fig. 1.1

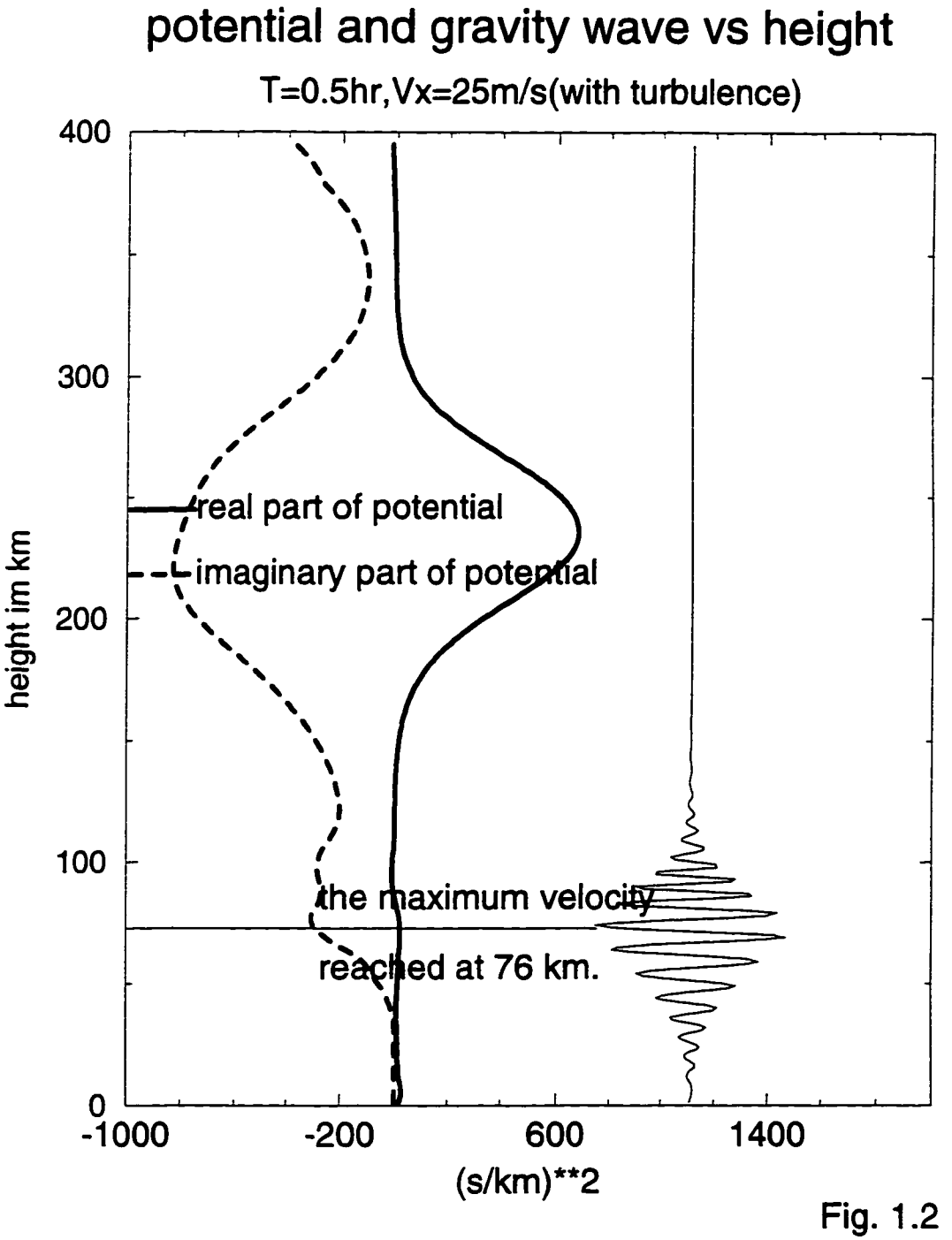

Fig. 1.2

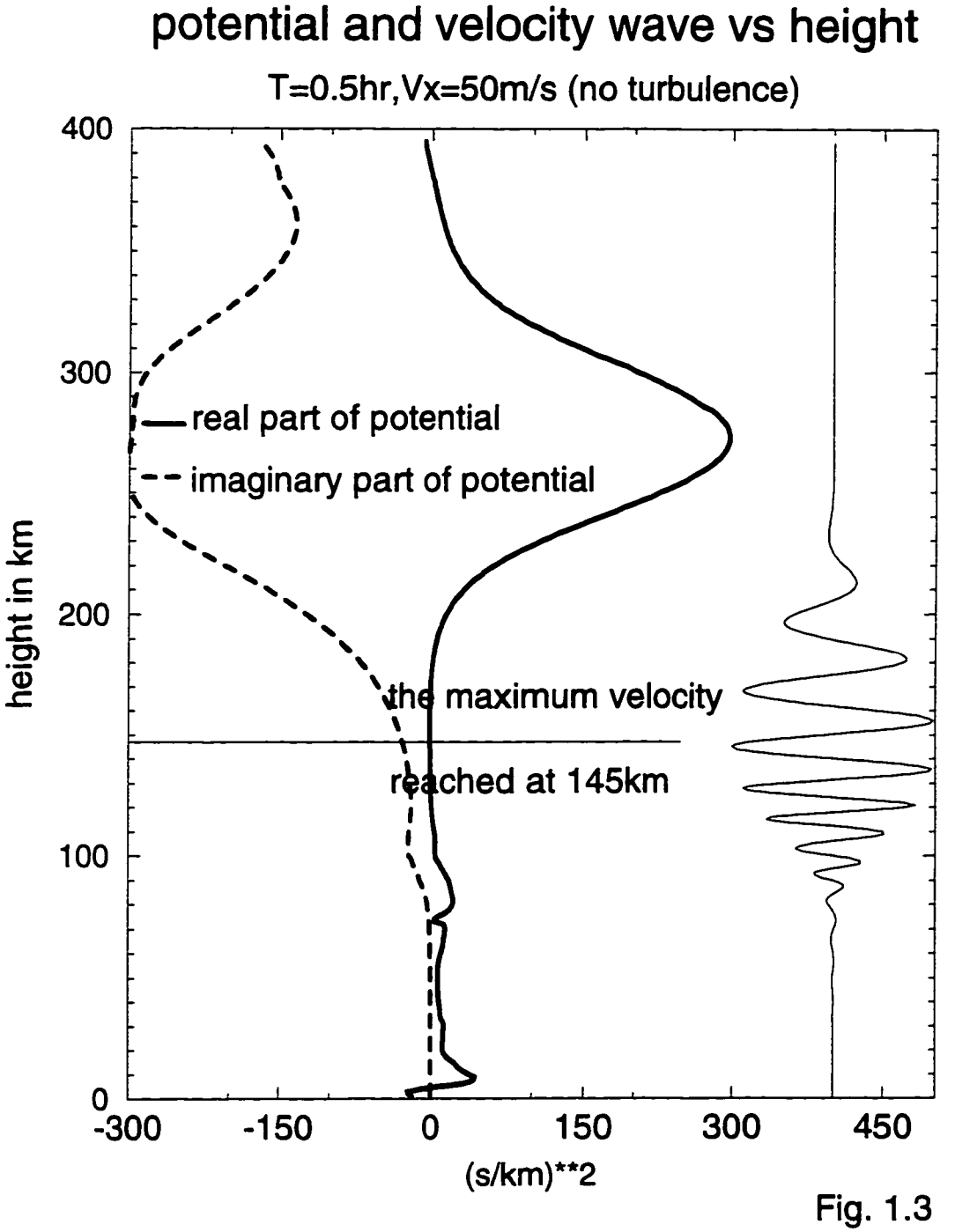

Fig. 1.3

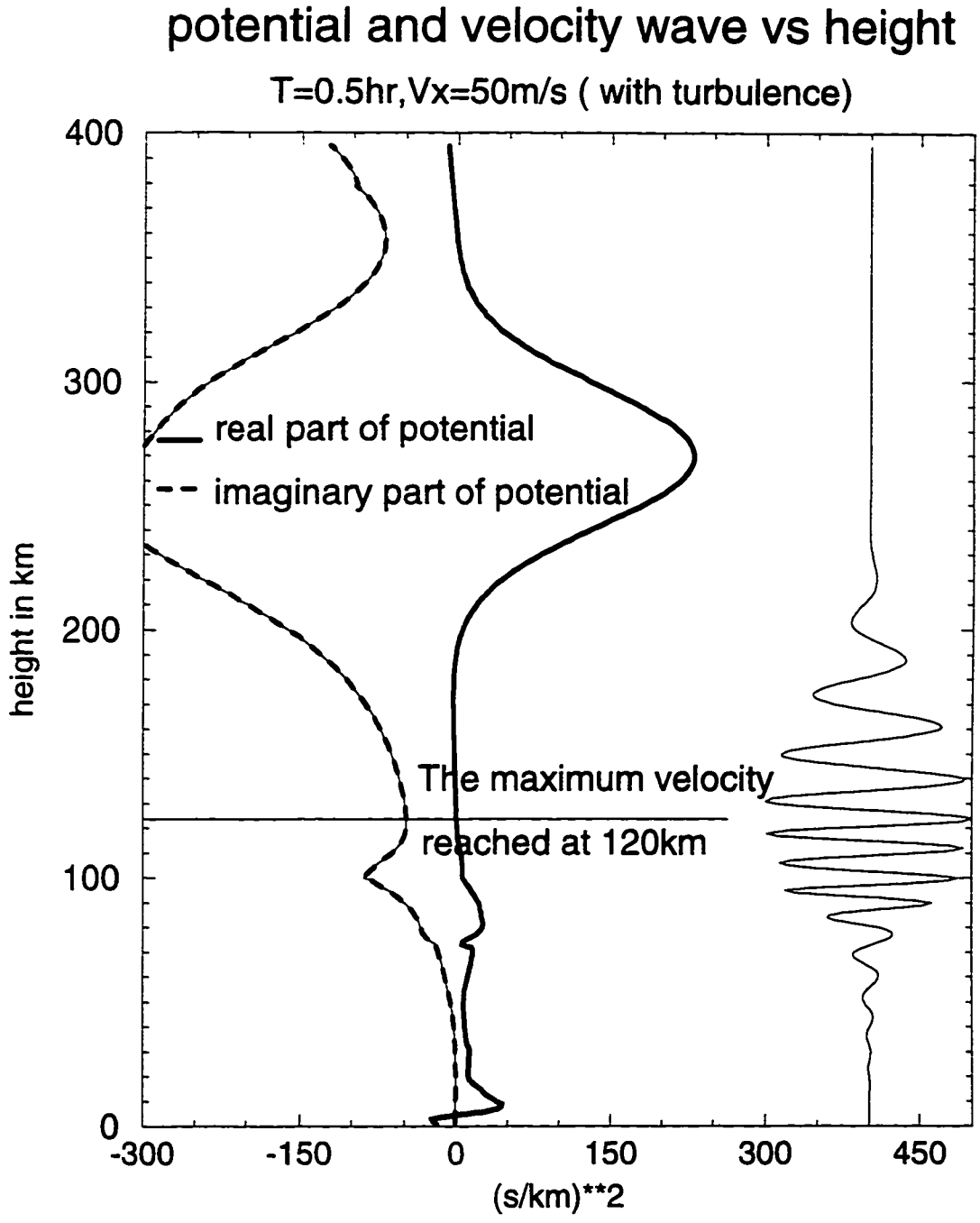

Fig. 1.4

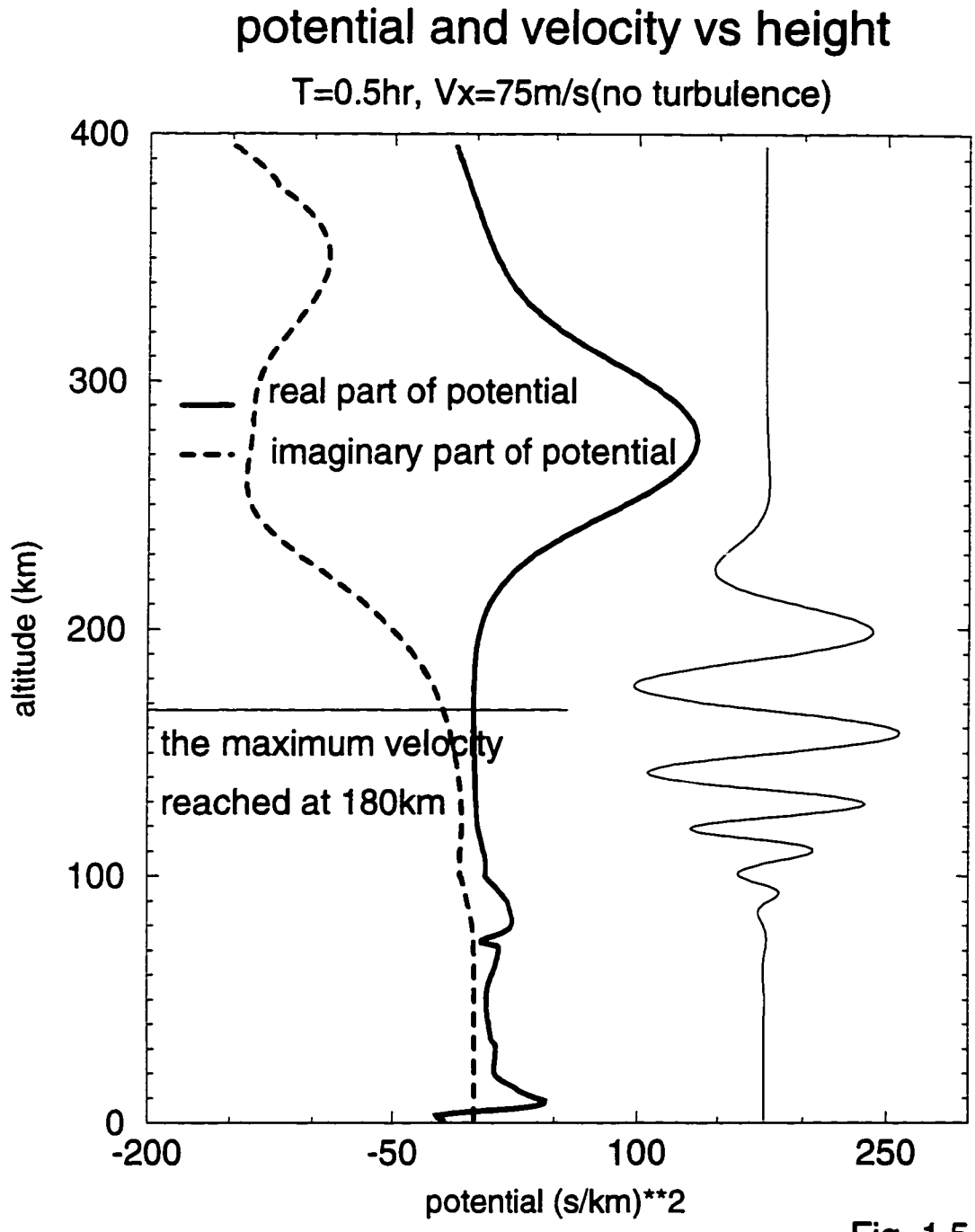

Fig. 1.5

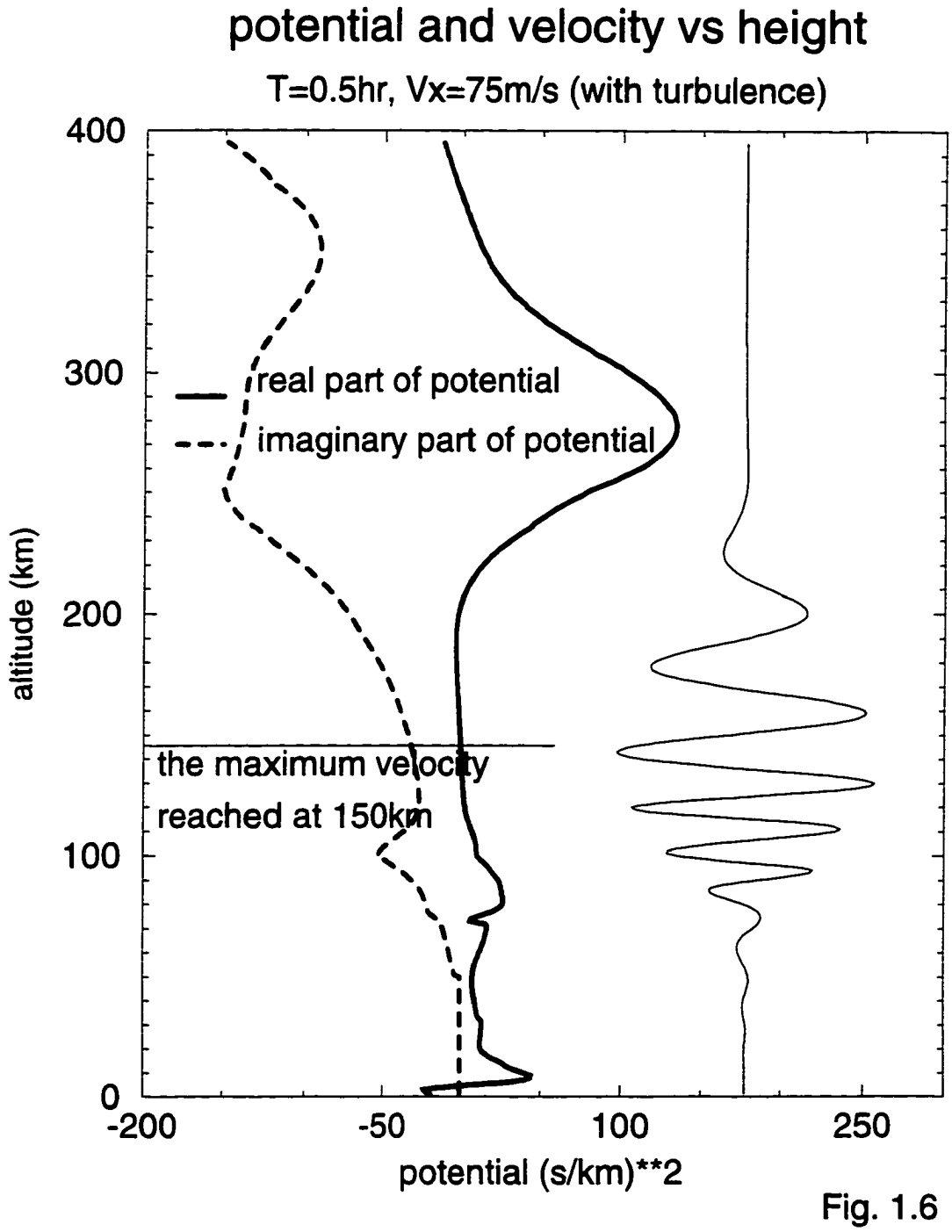

Fig. 1.6

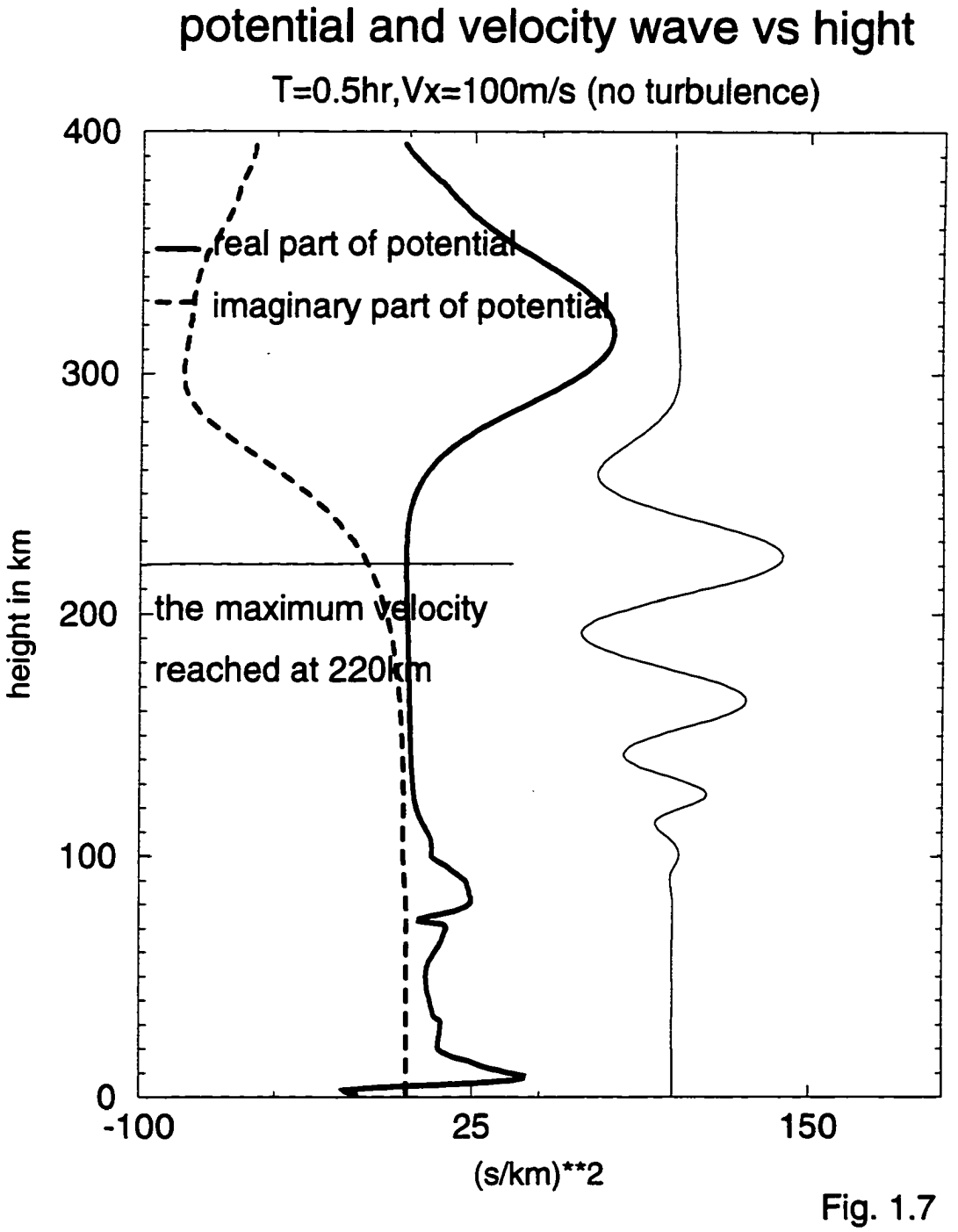

Fig. 1.7

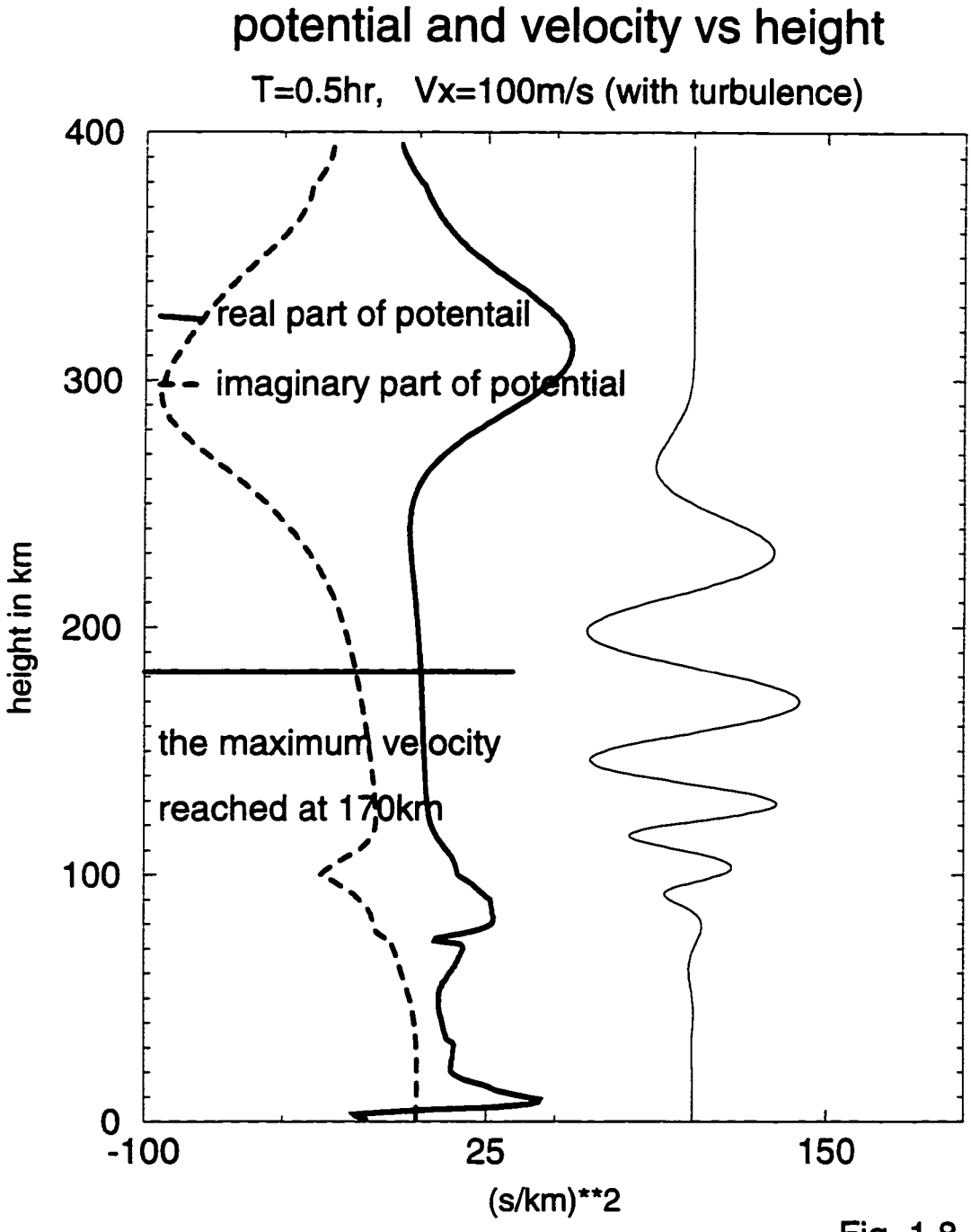

Fig. 1.8

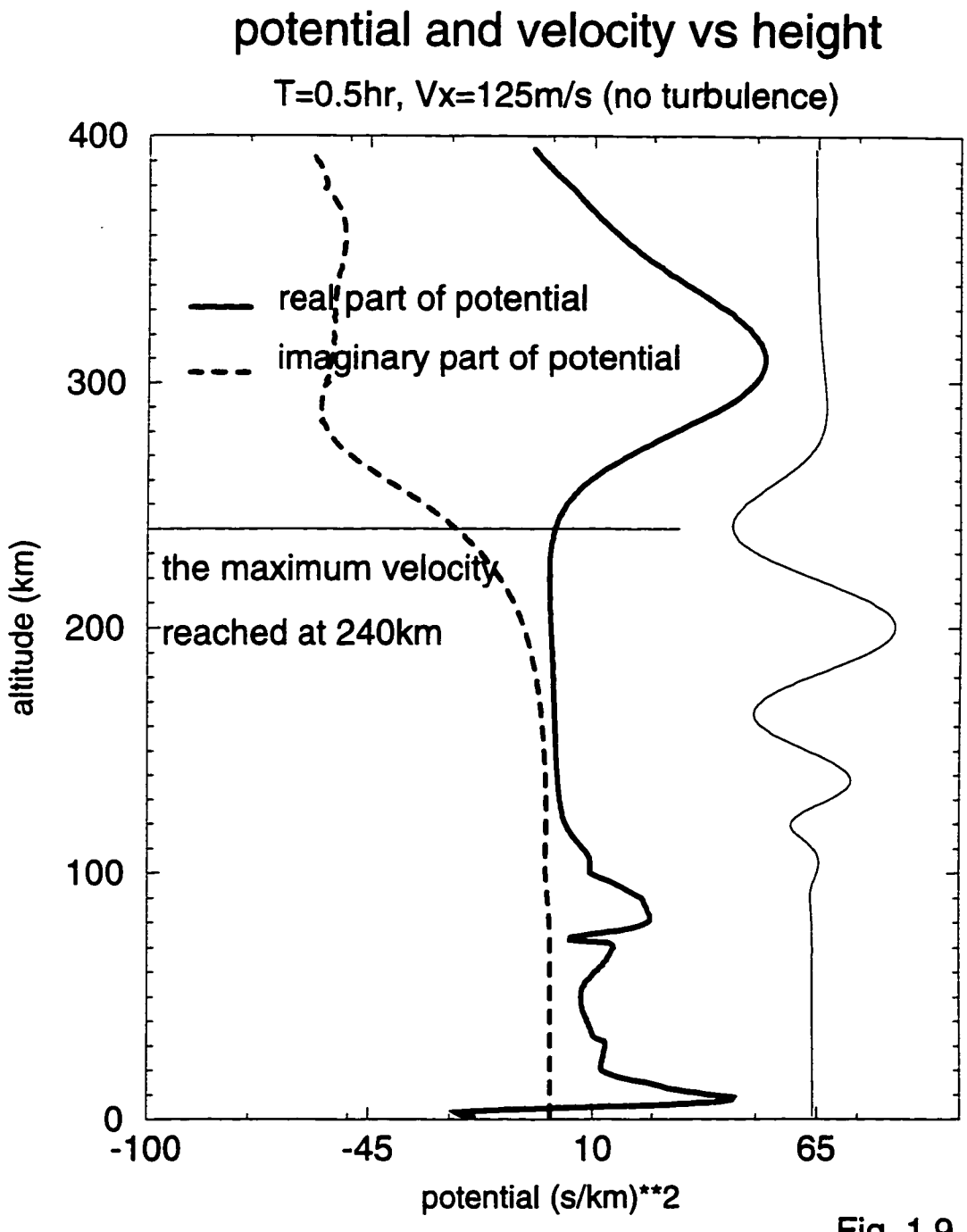

Fig. 1.9

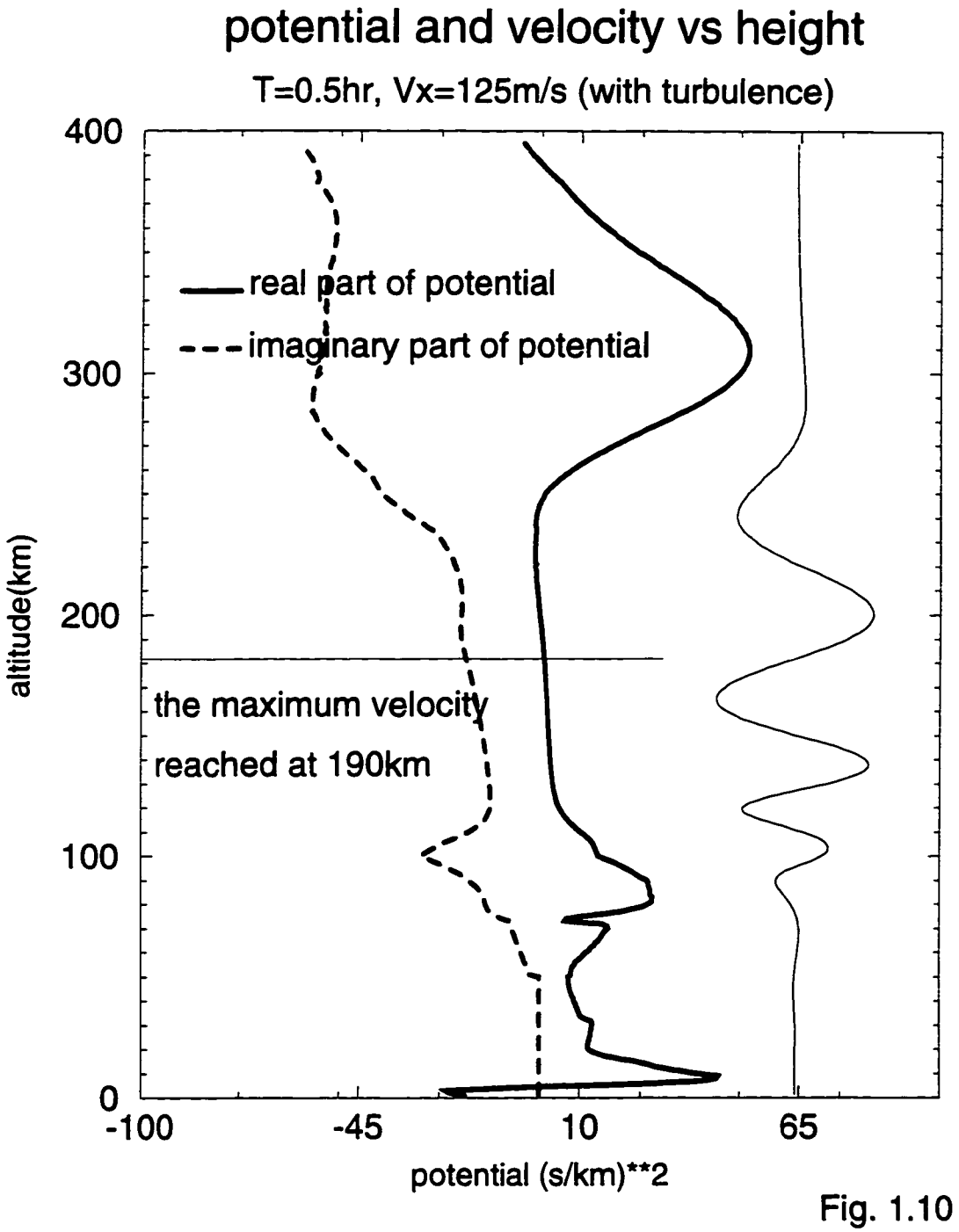

Fig. 1.10

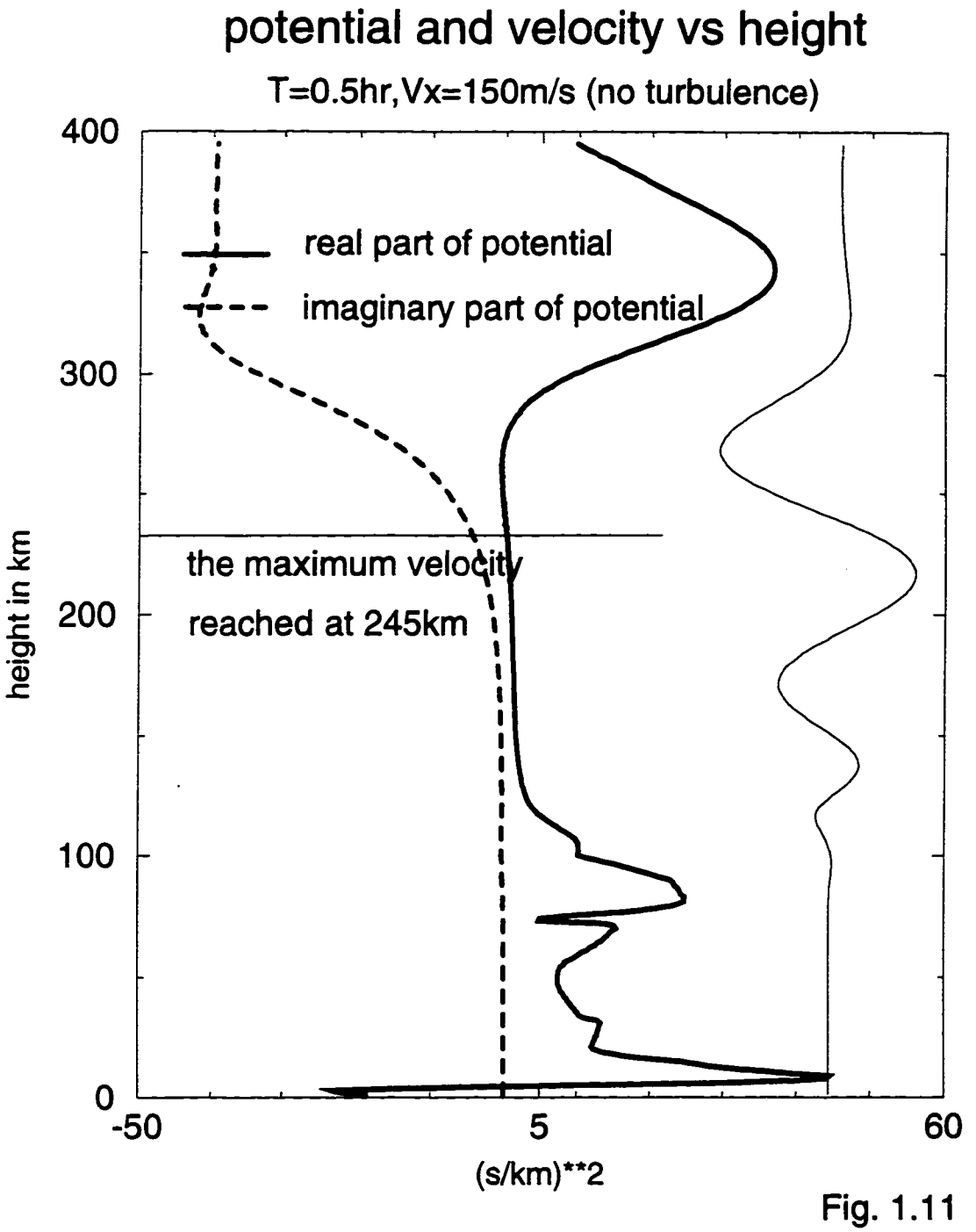

Fig. 1.11

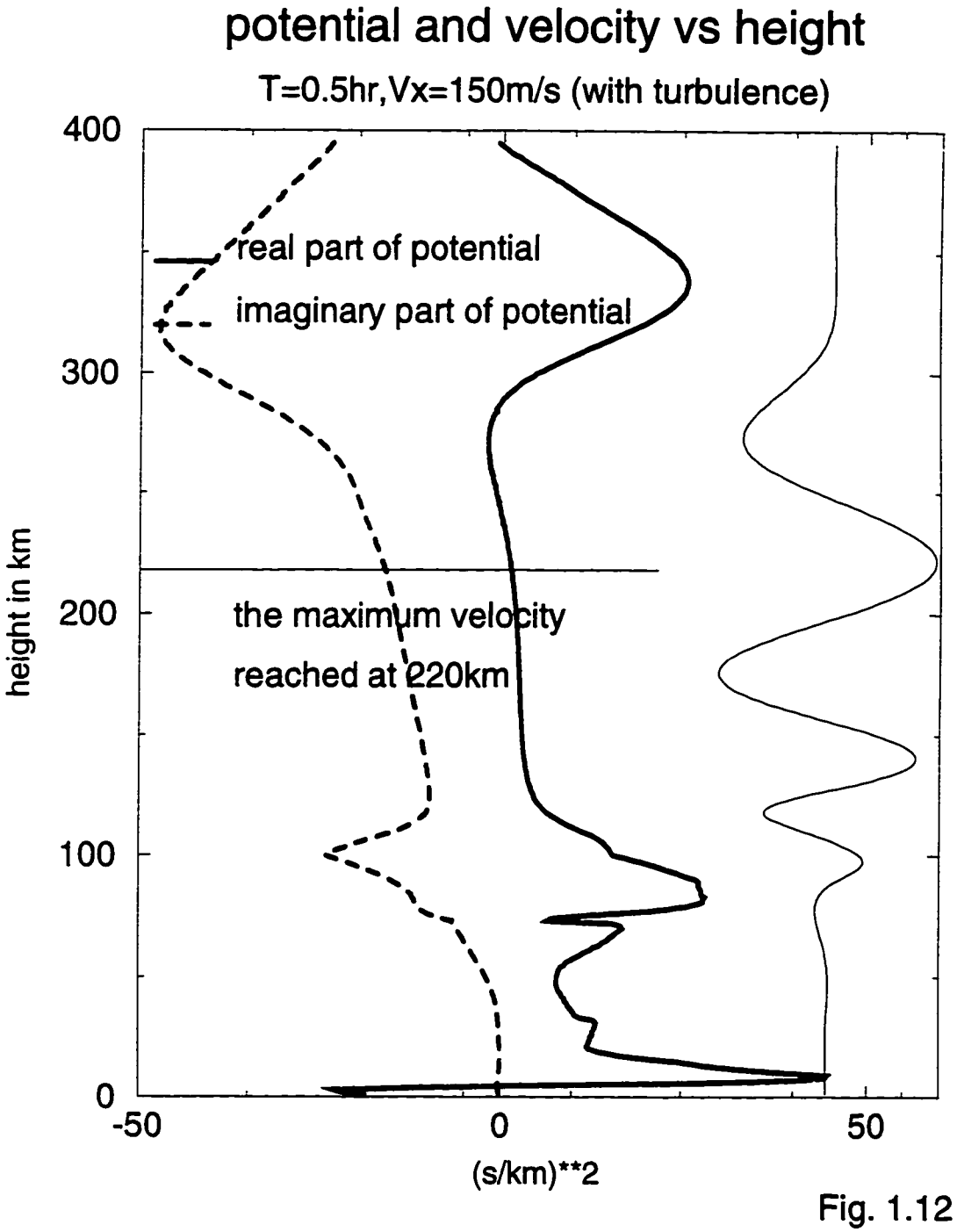

Fig. 1.12

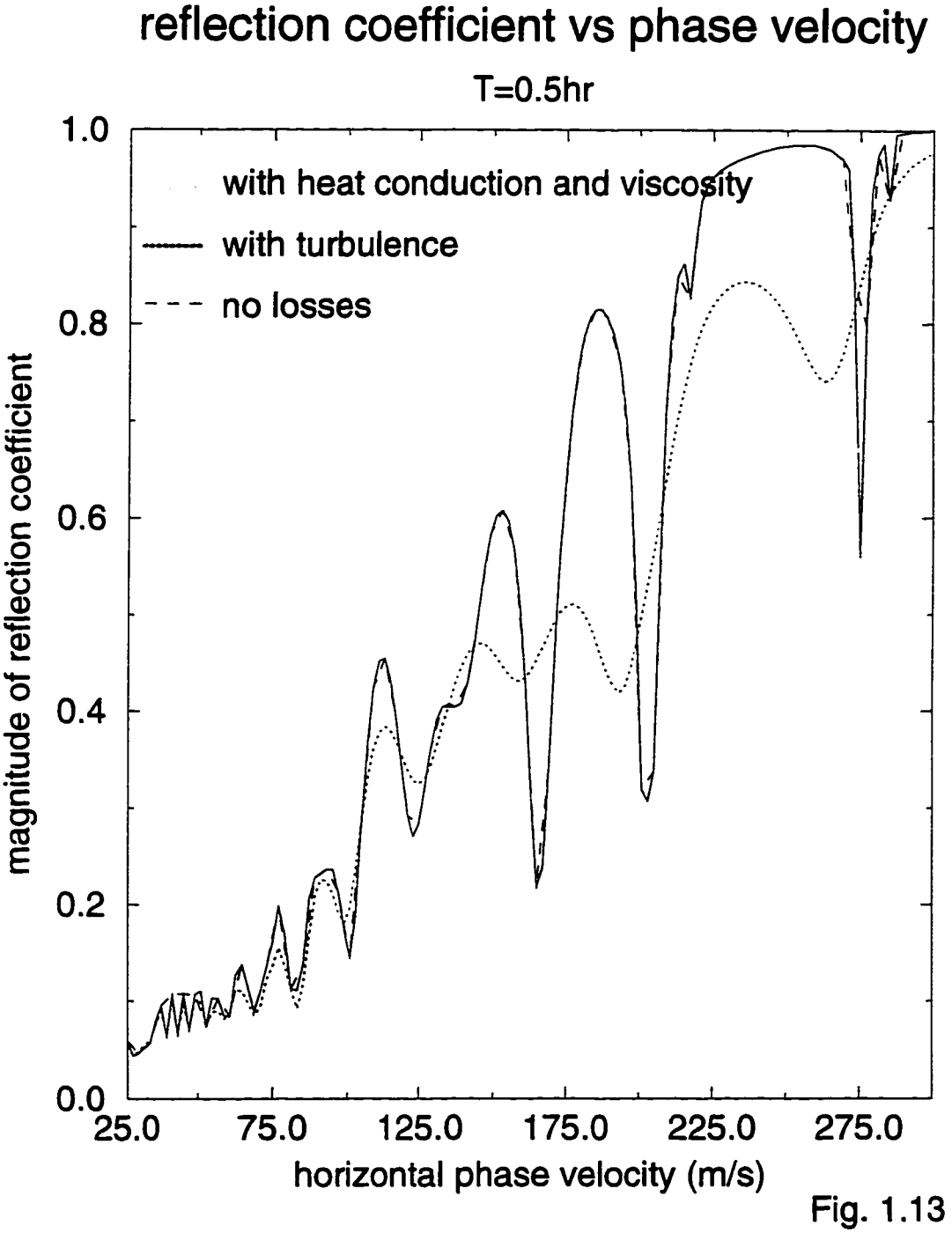

Fig. 1.13

(T=0.5hr, Vx=185m/s)

potential(s/km)**2

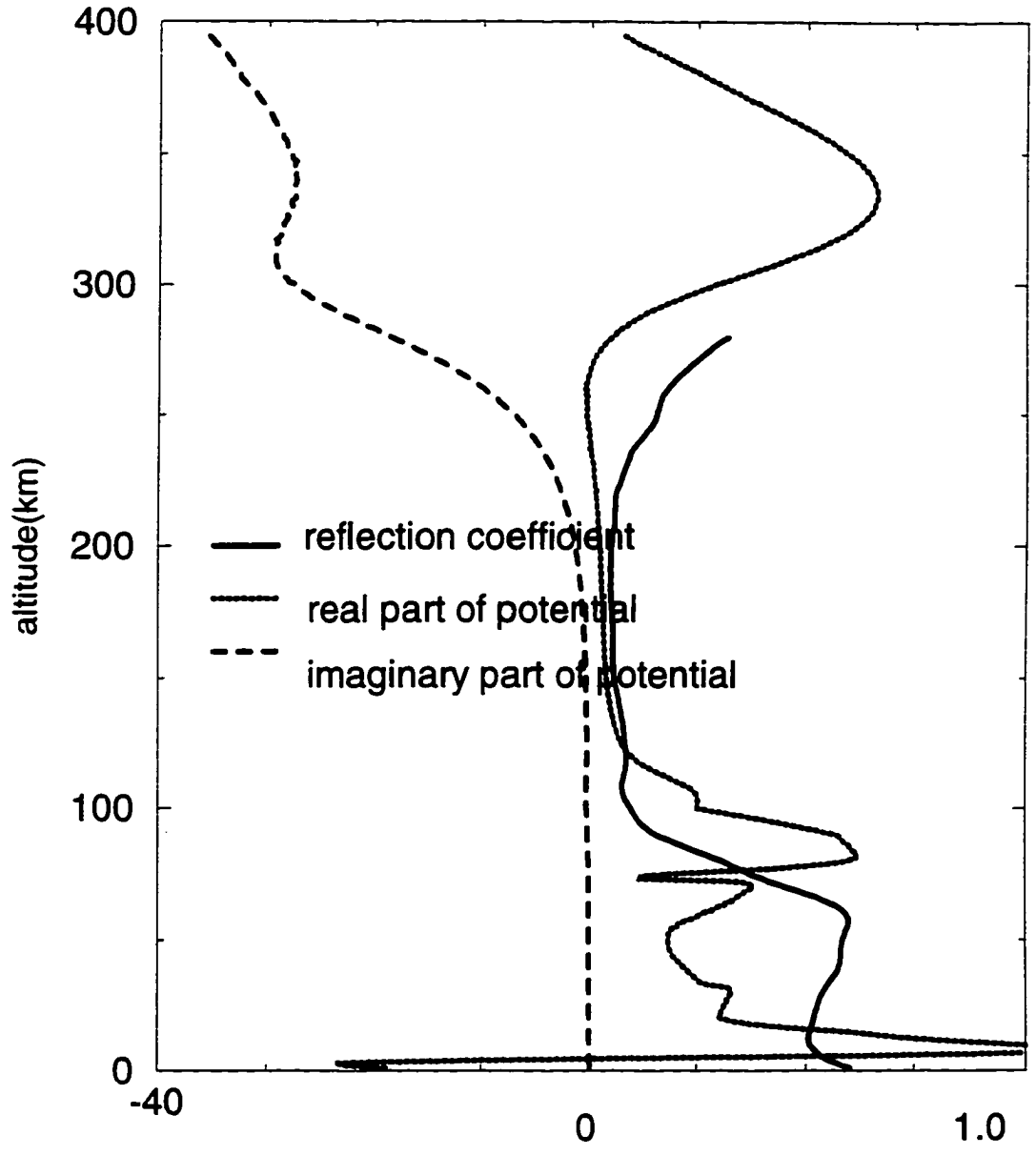

Fig. 1.14

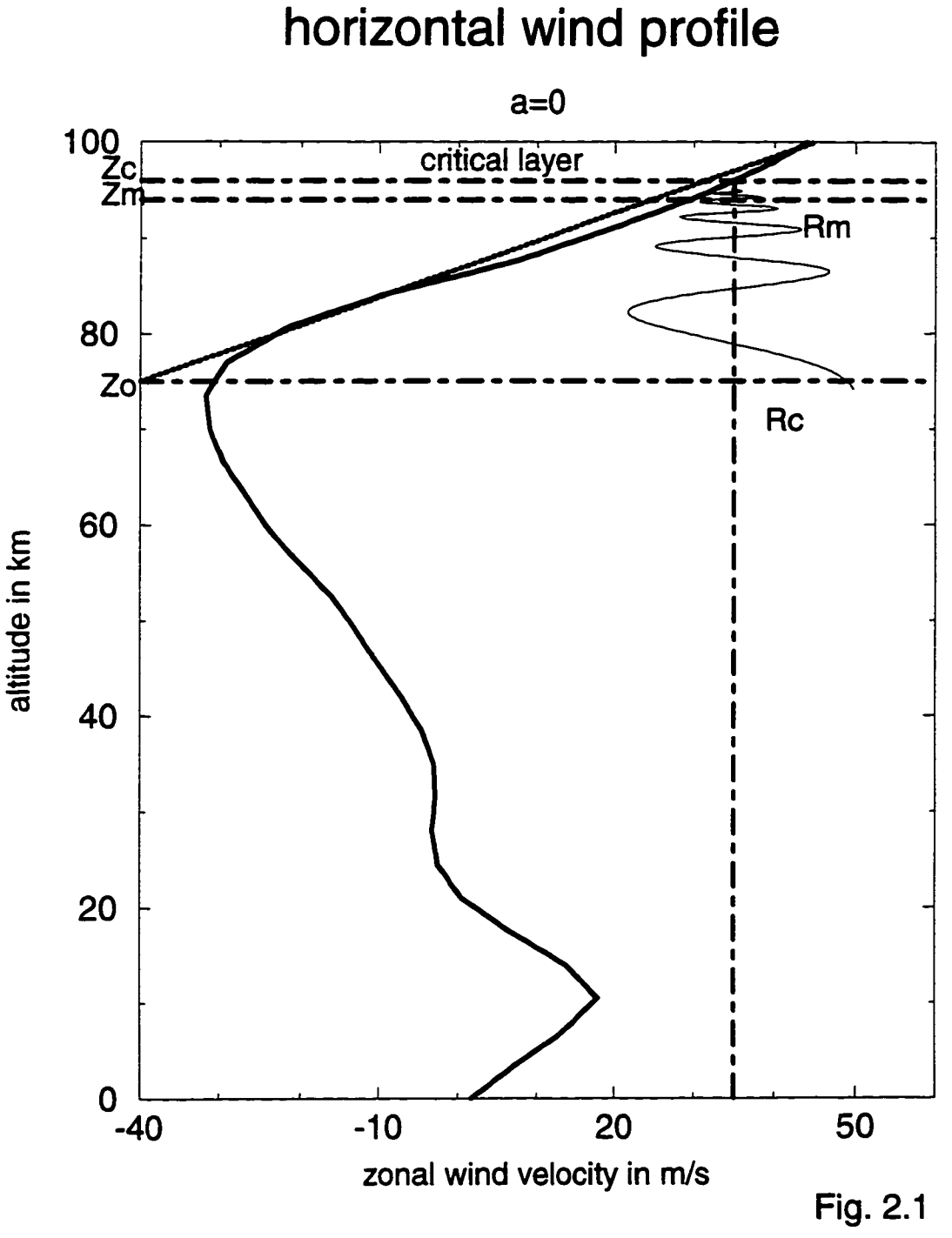

Fig. 2.1

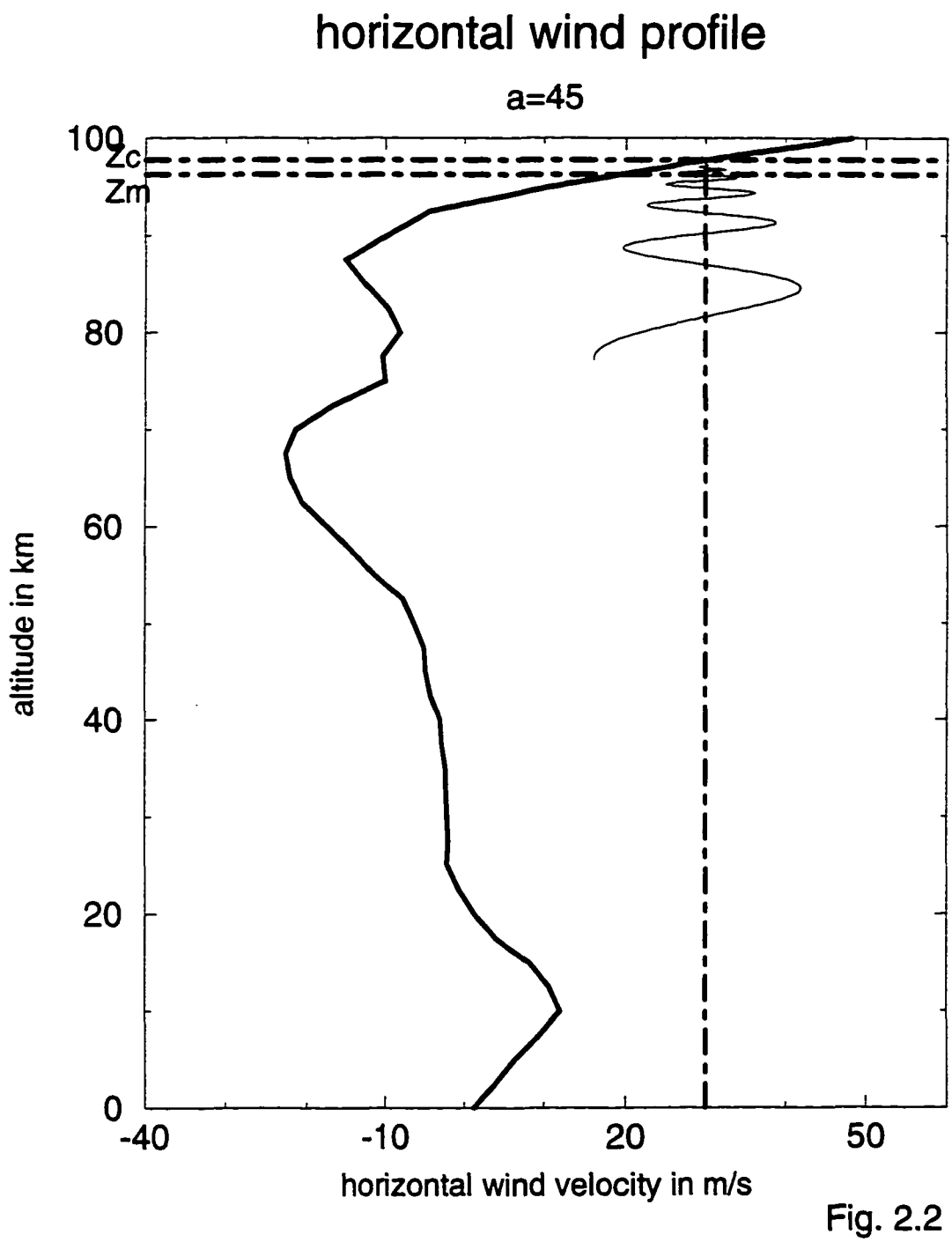

Fig. 2.2

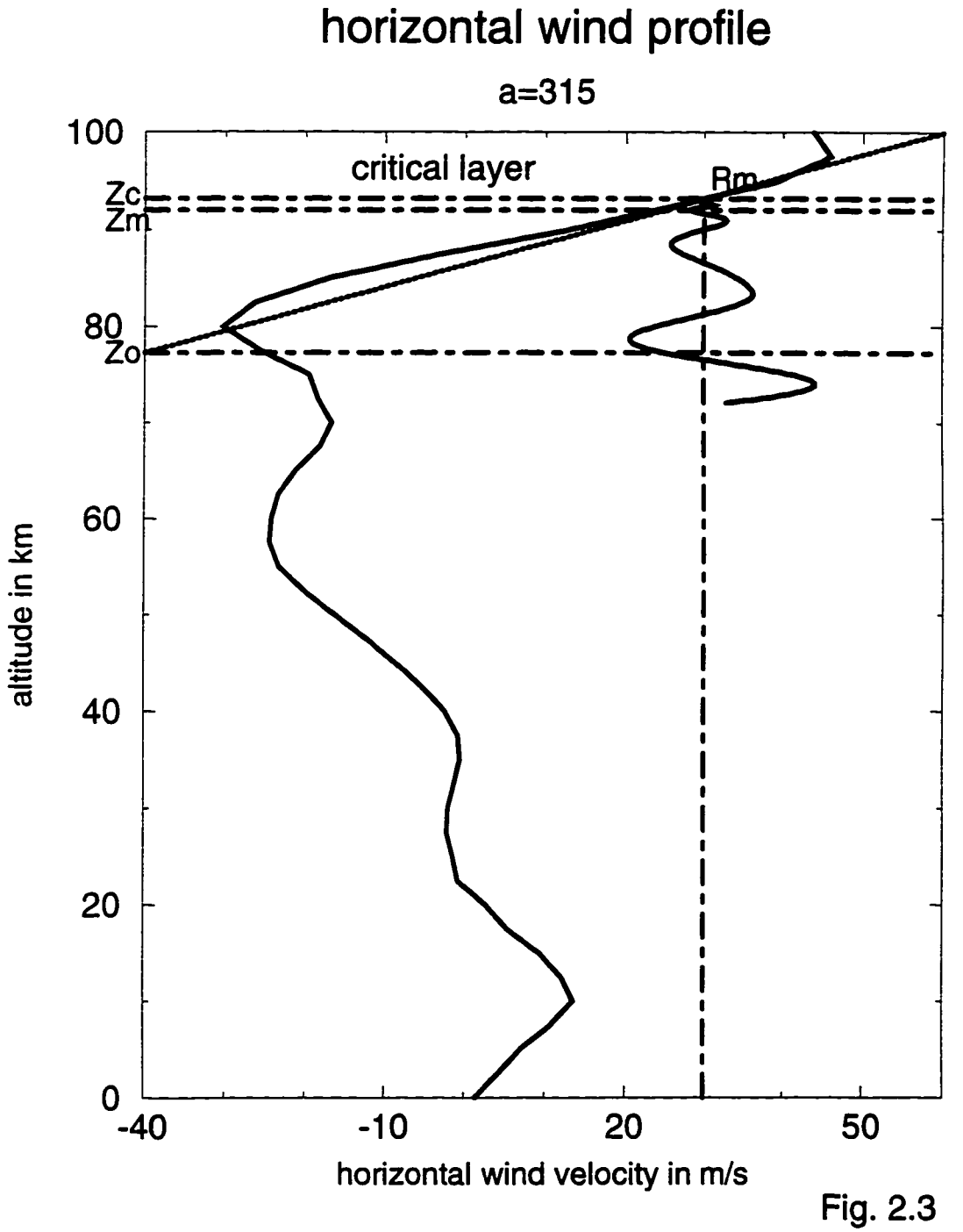

Fig. 2.3

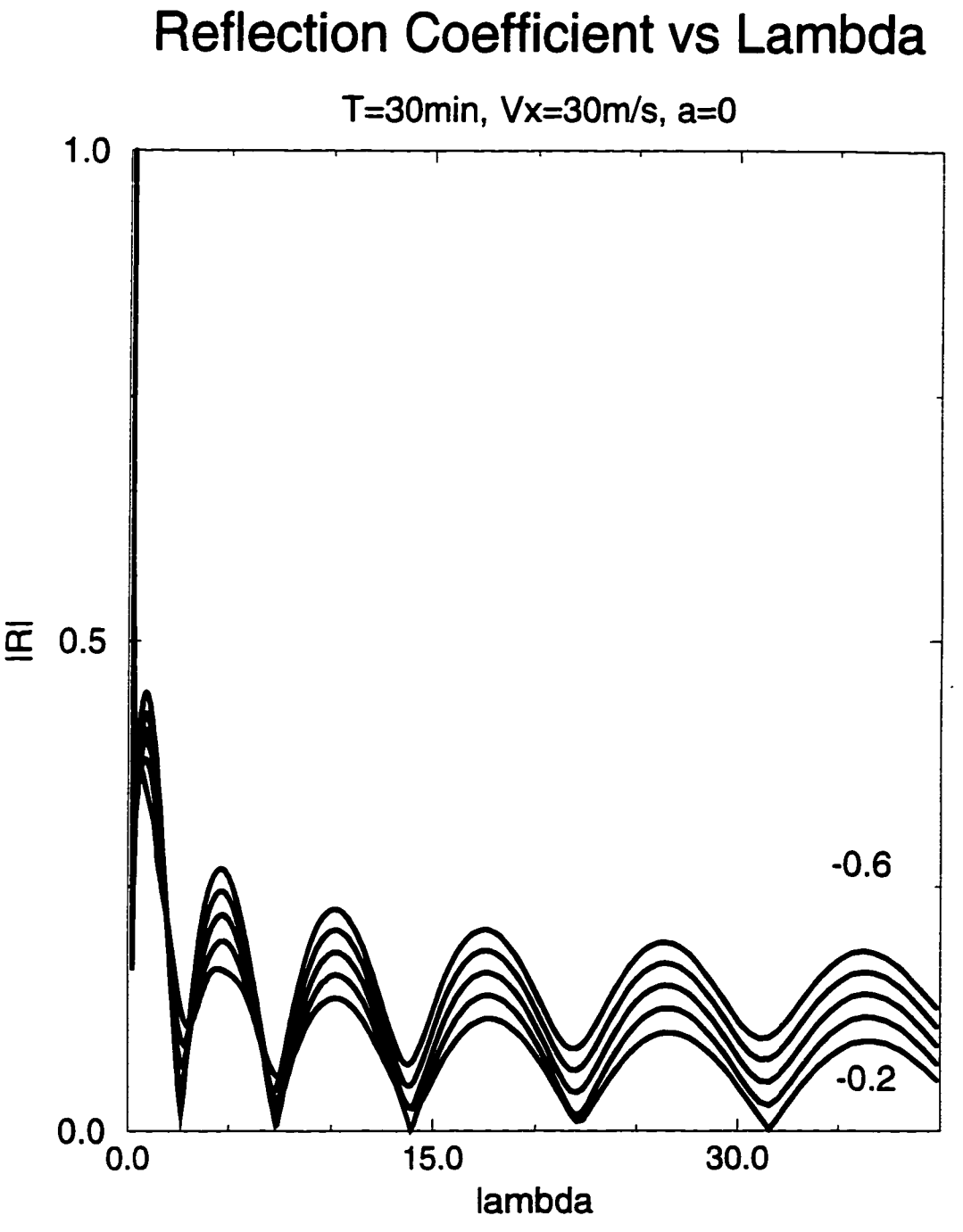

Fig. 2.4

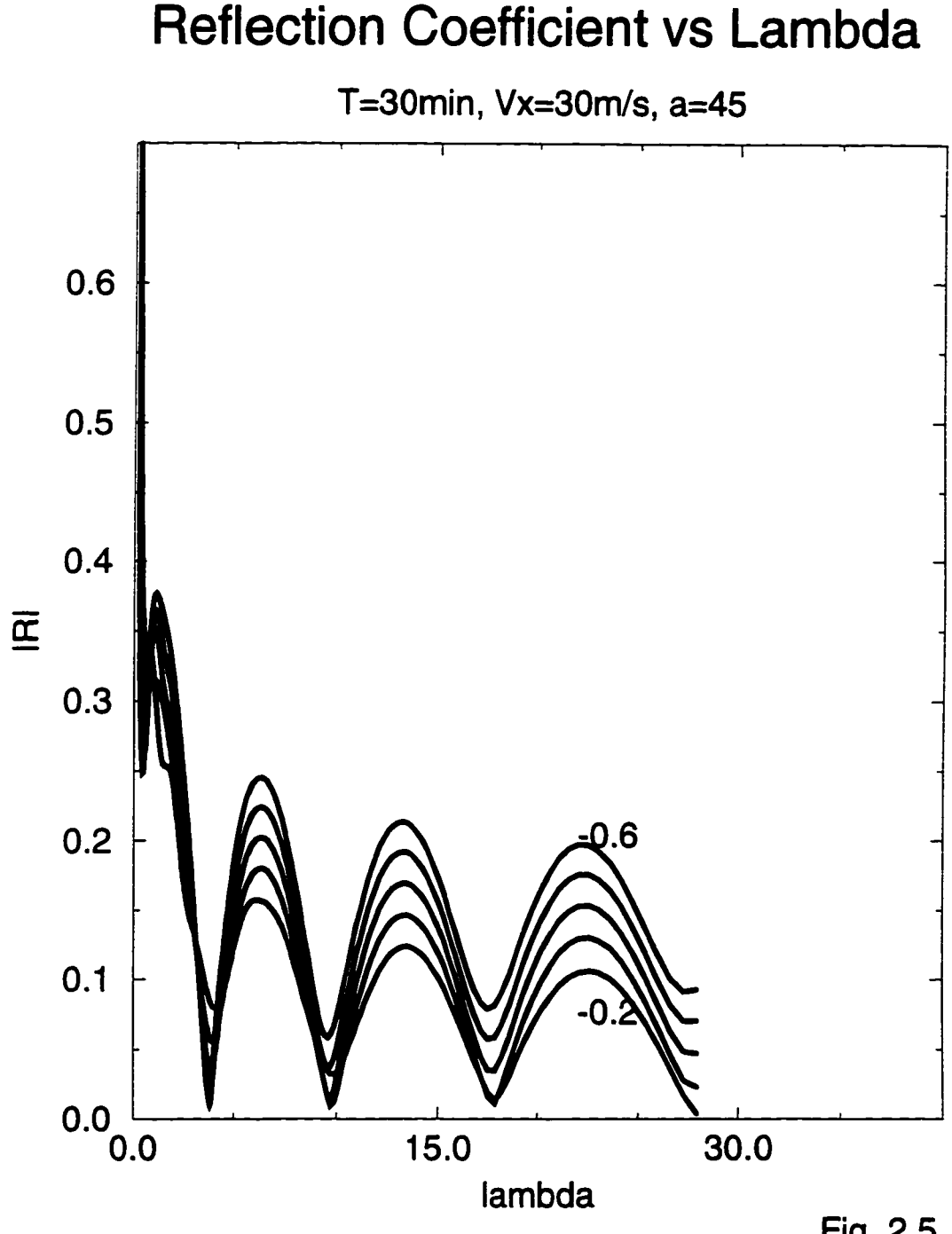

Fig. 2.5

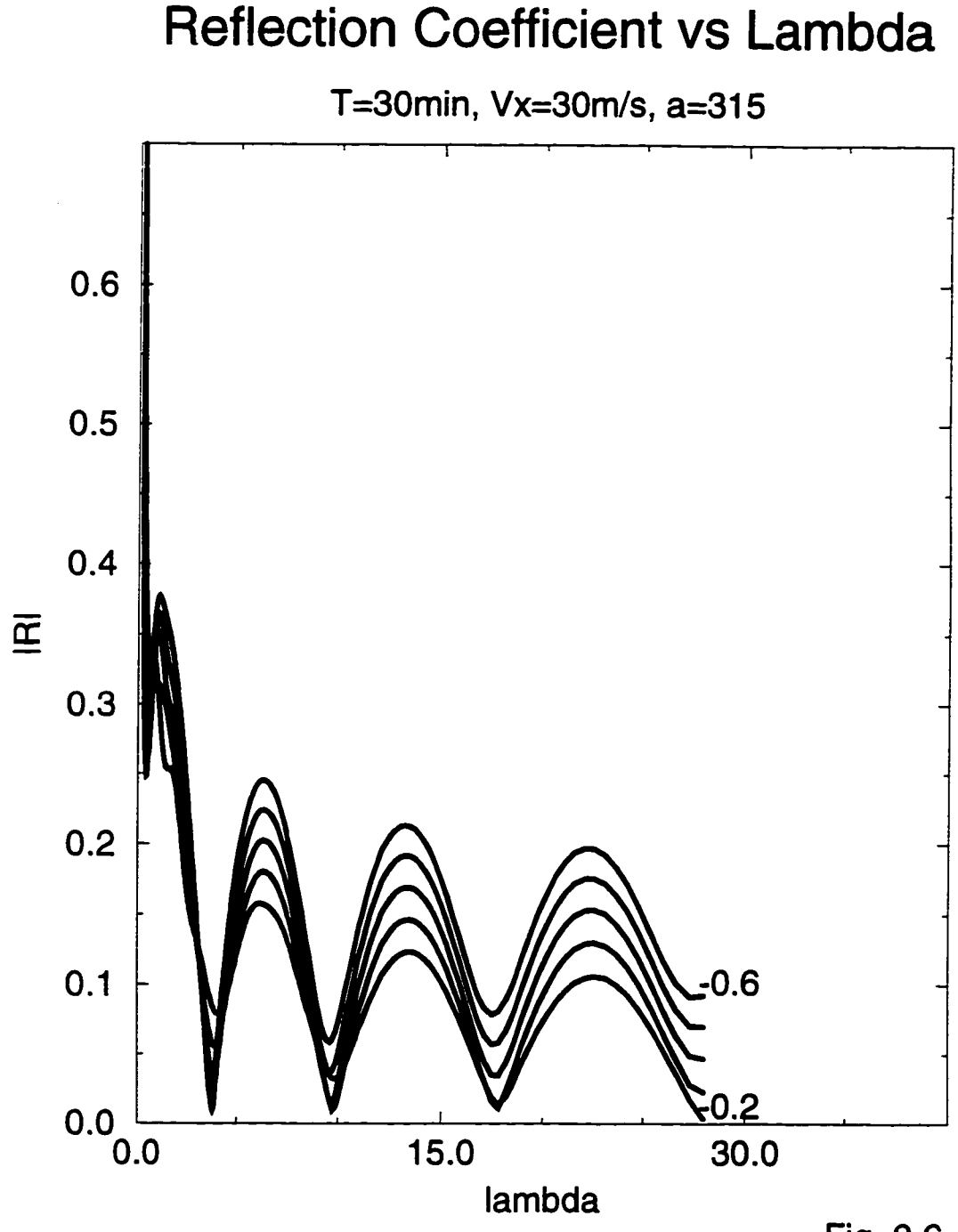

Fig. 2.6

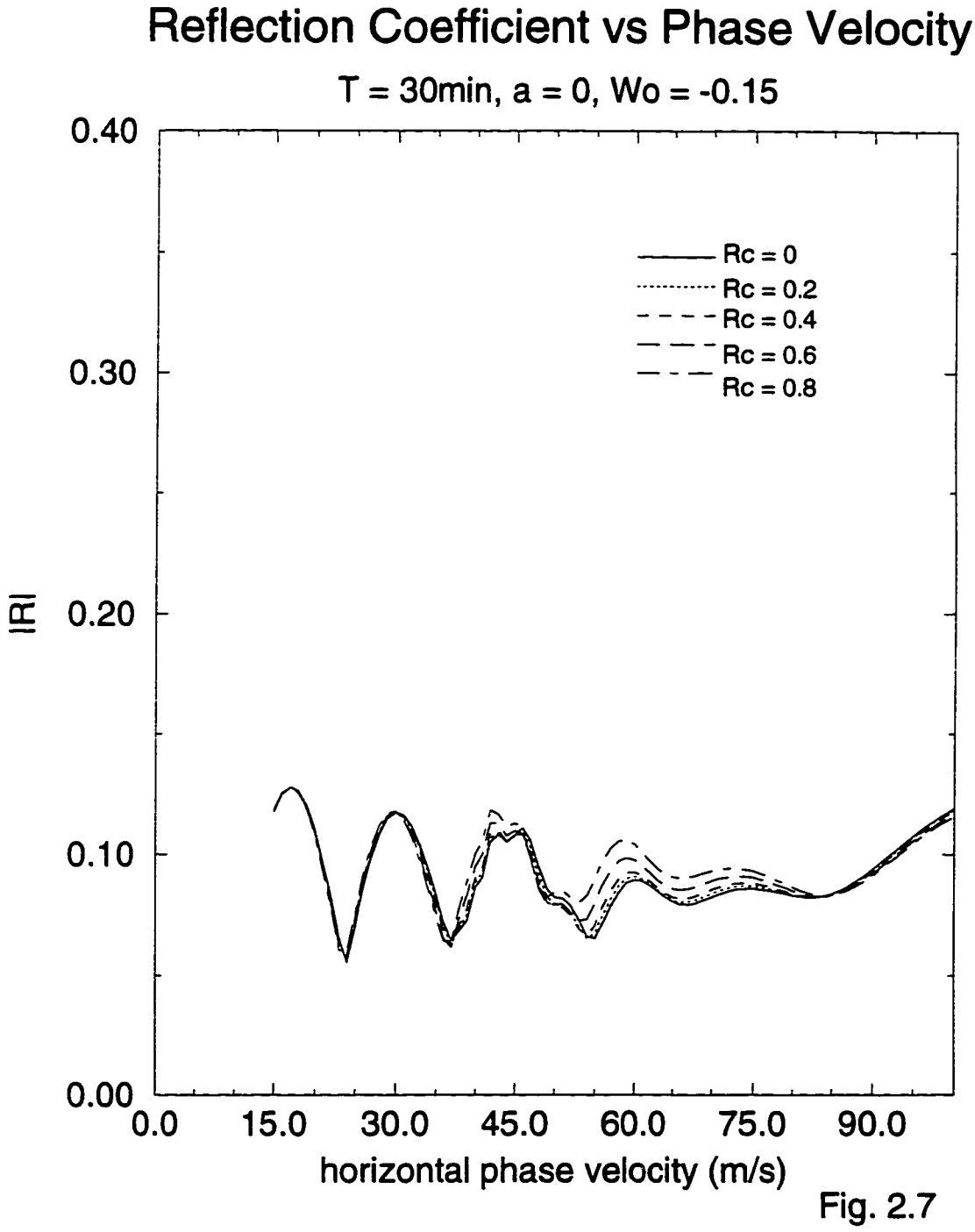

Fig. 2.7

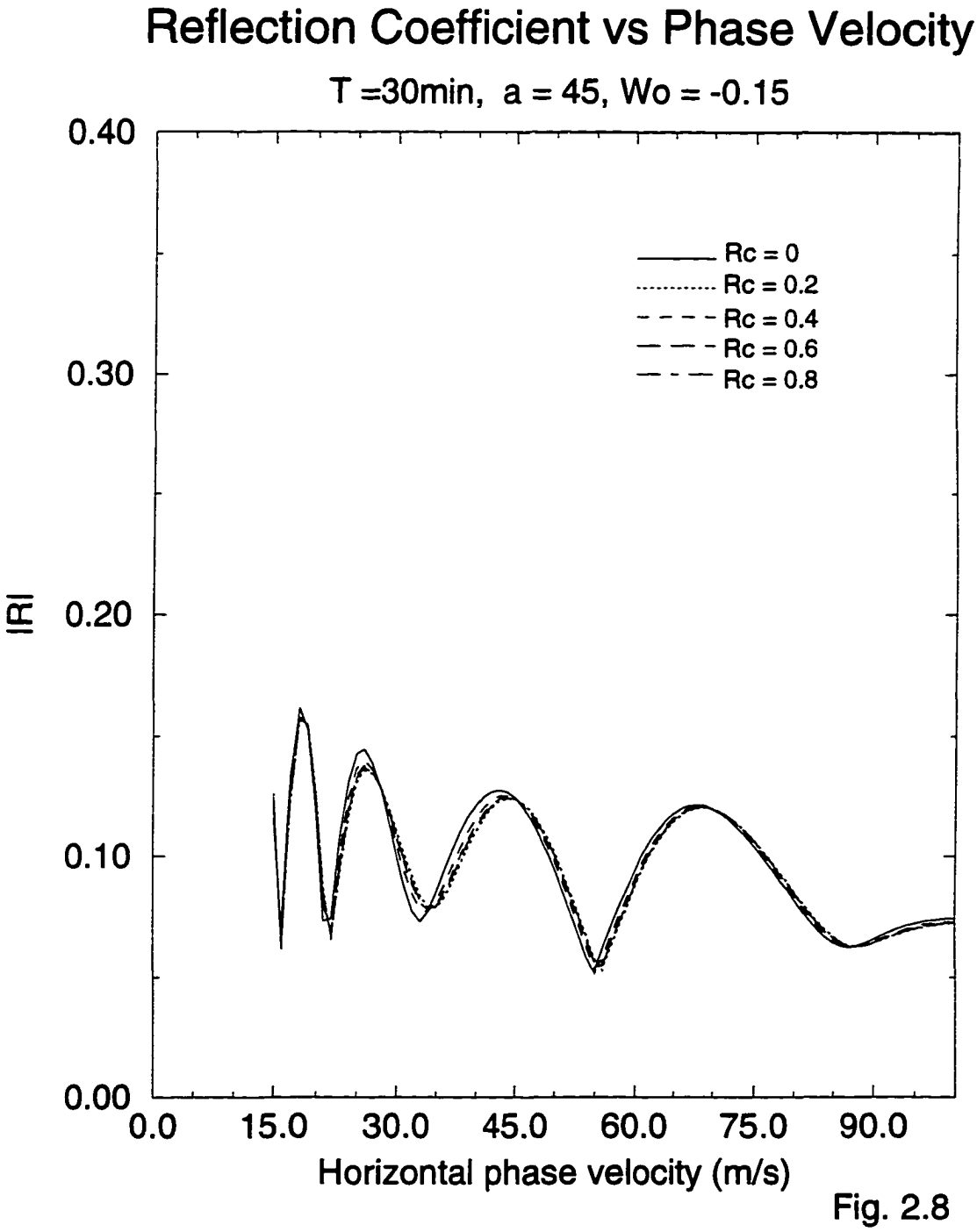

Fig. 2.8

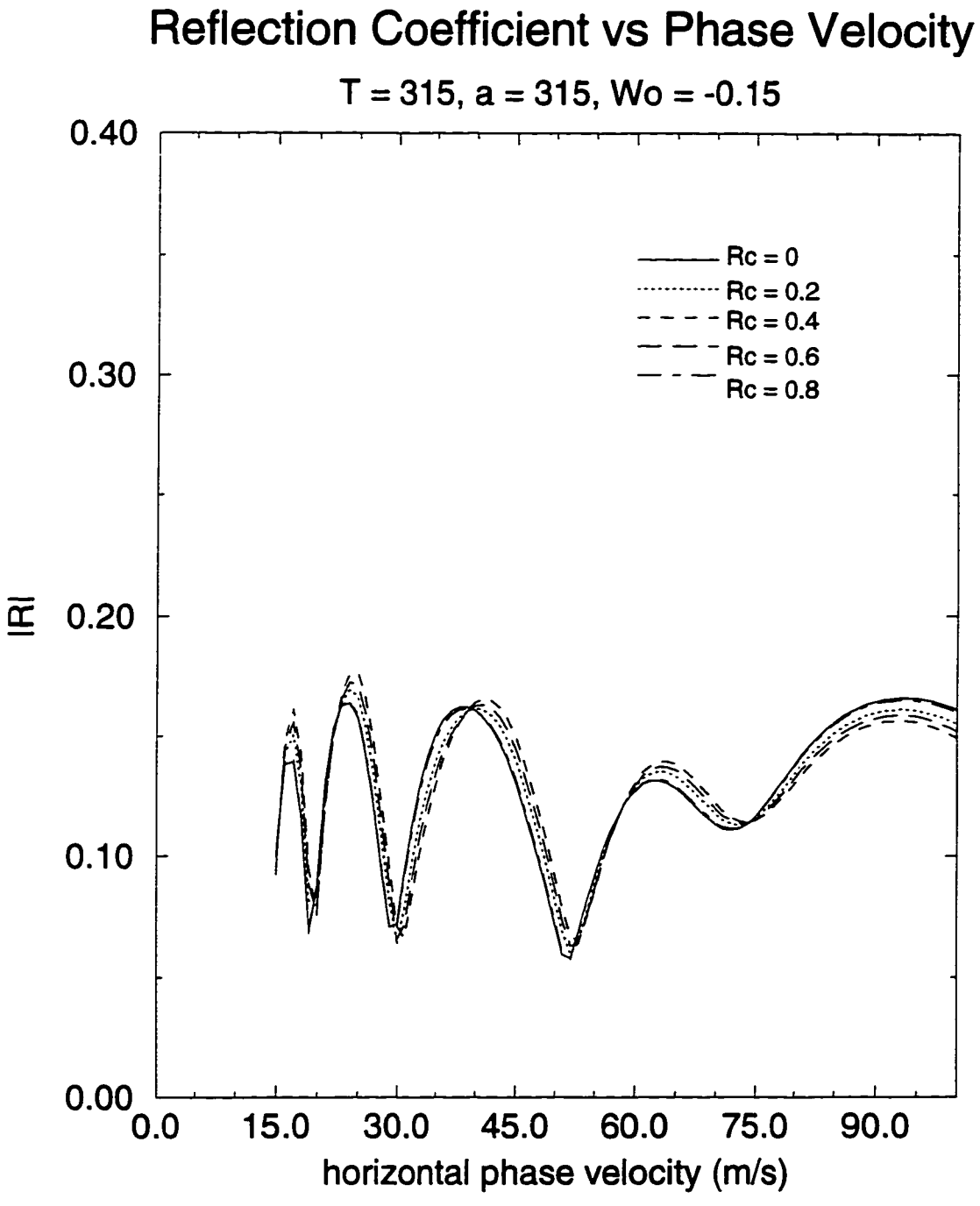

Fig. 2.9

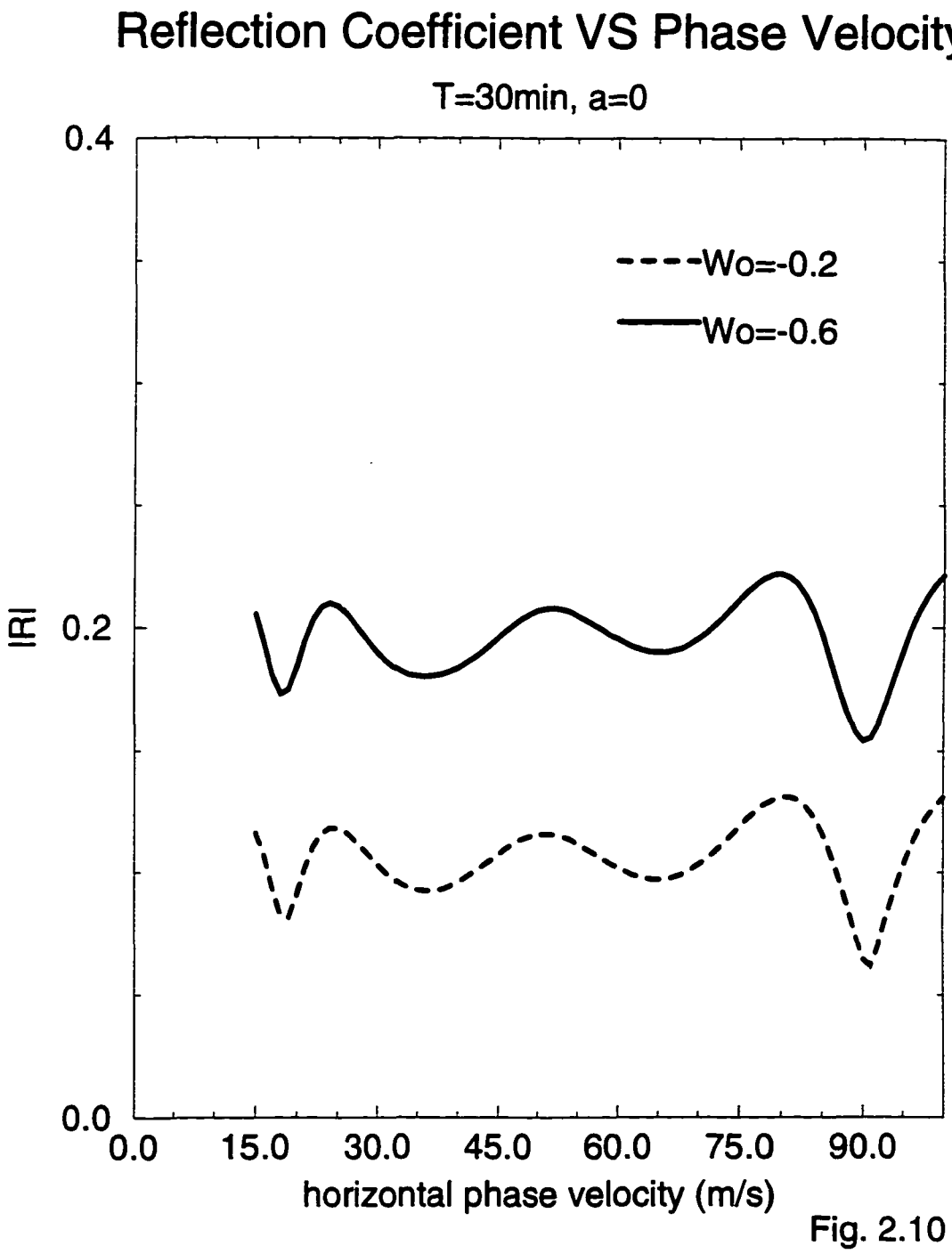

Fig. 2.10

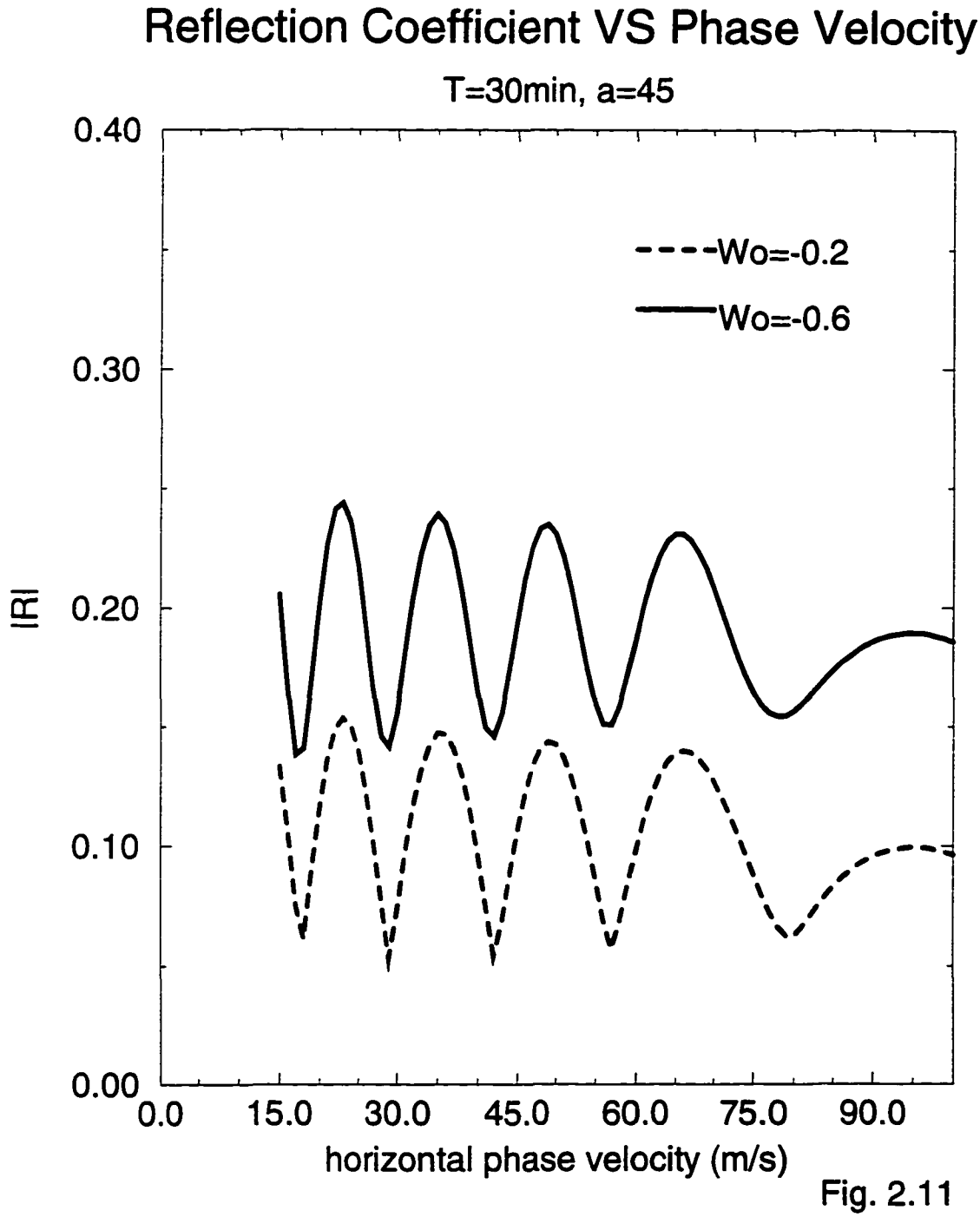

Fig. 2.11

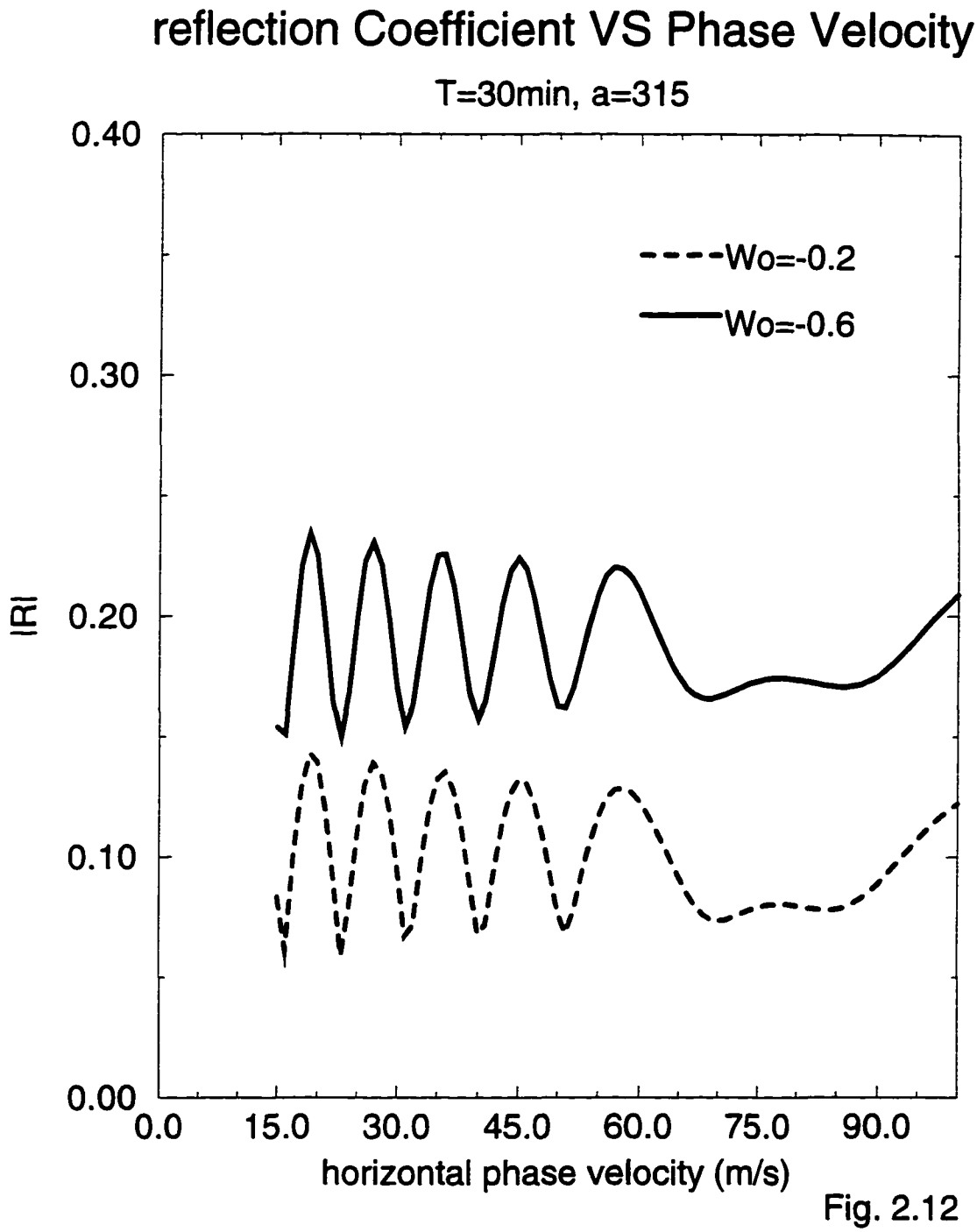

Fig. 2.12

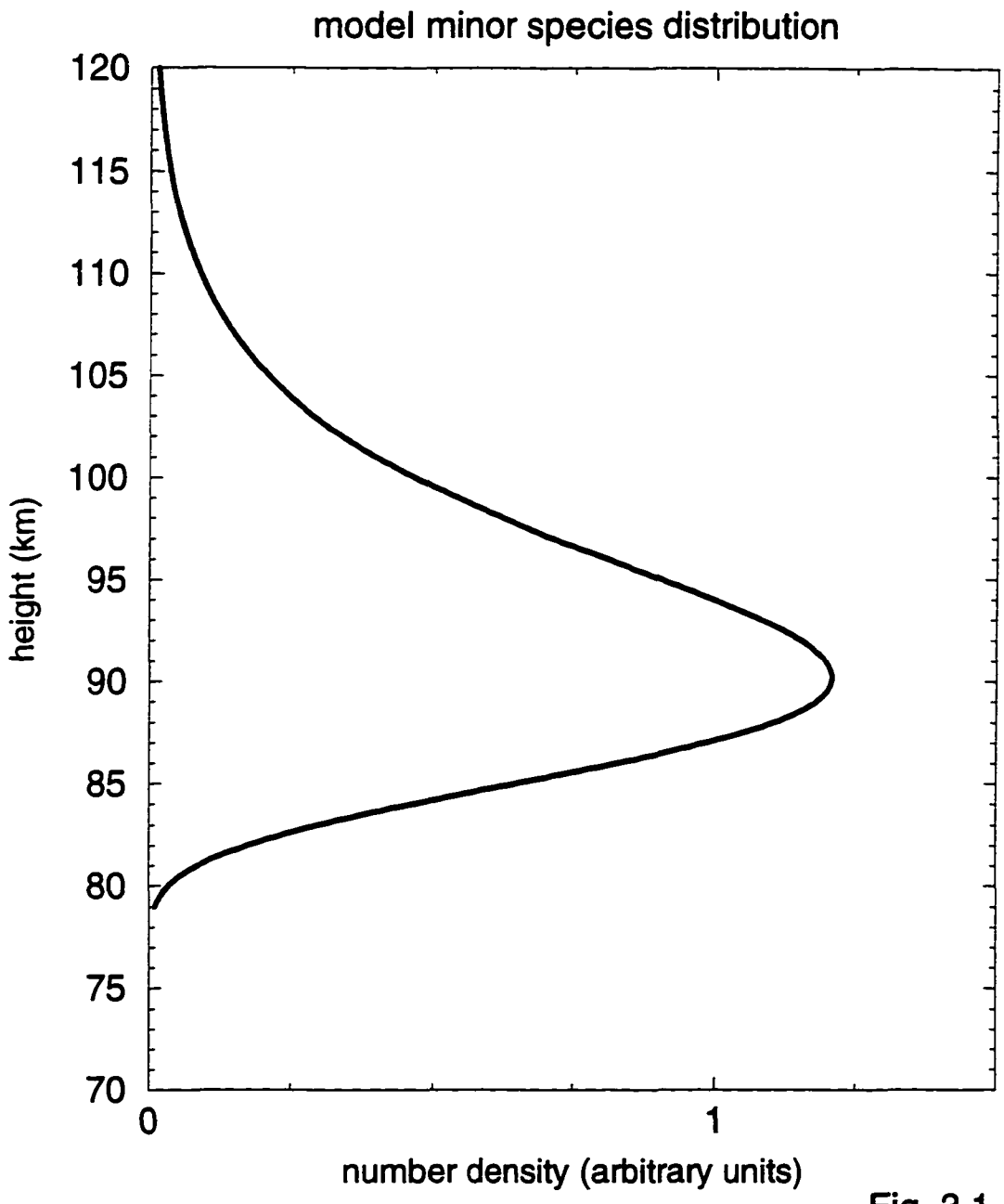

Fig. 3.1

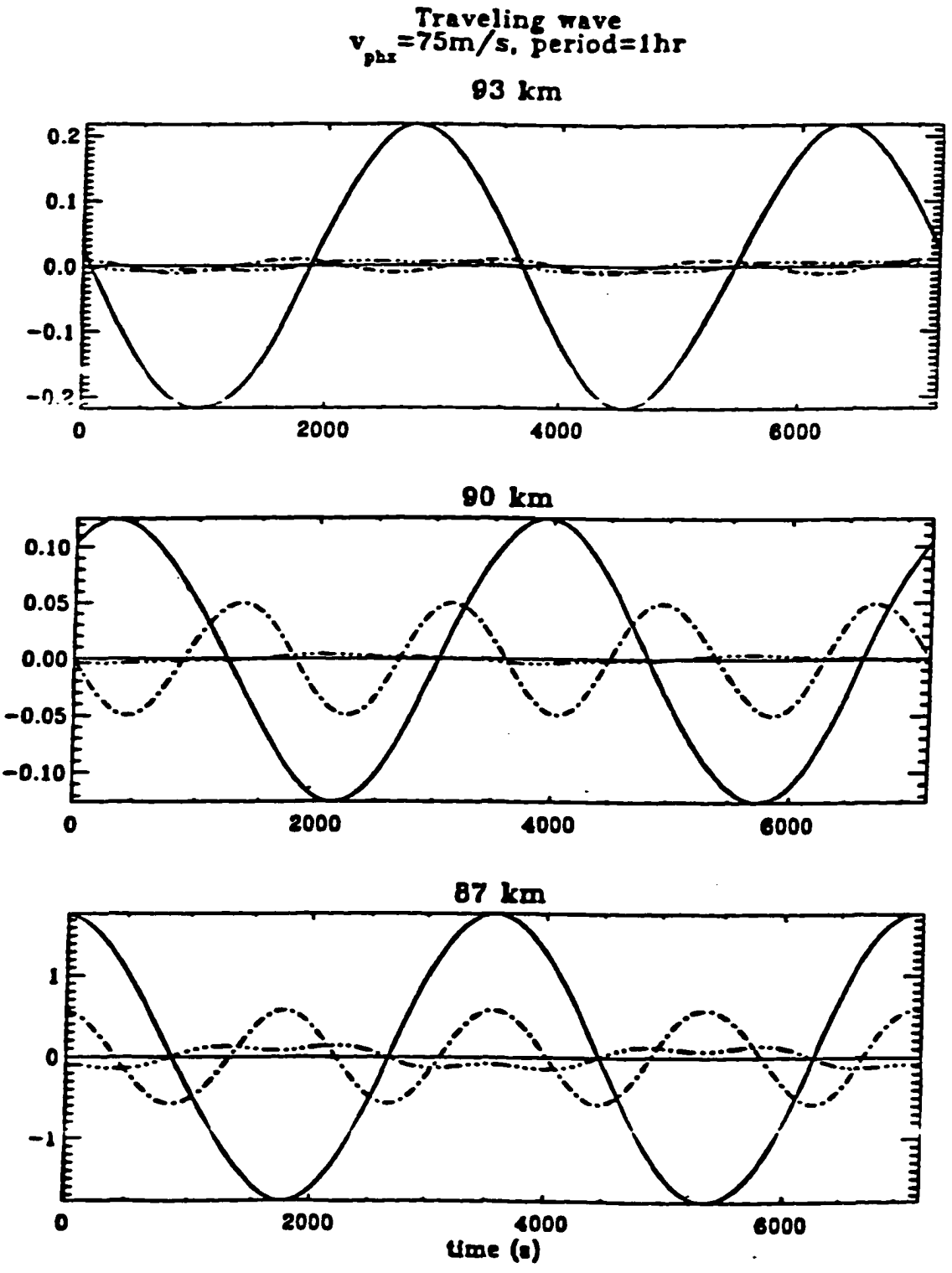

Fig. 3.2

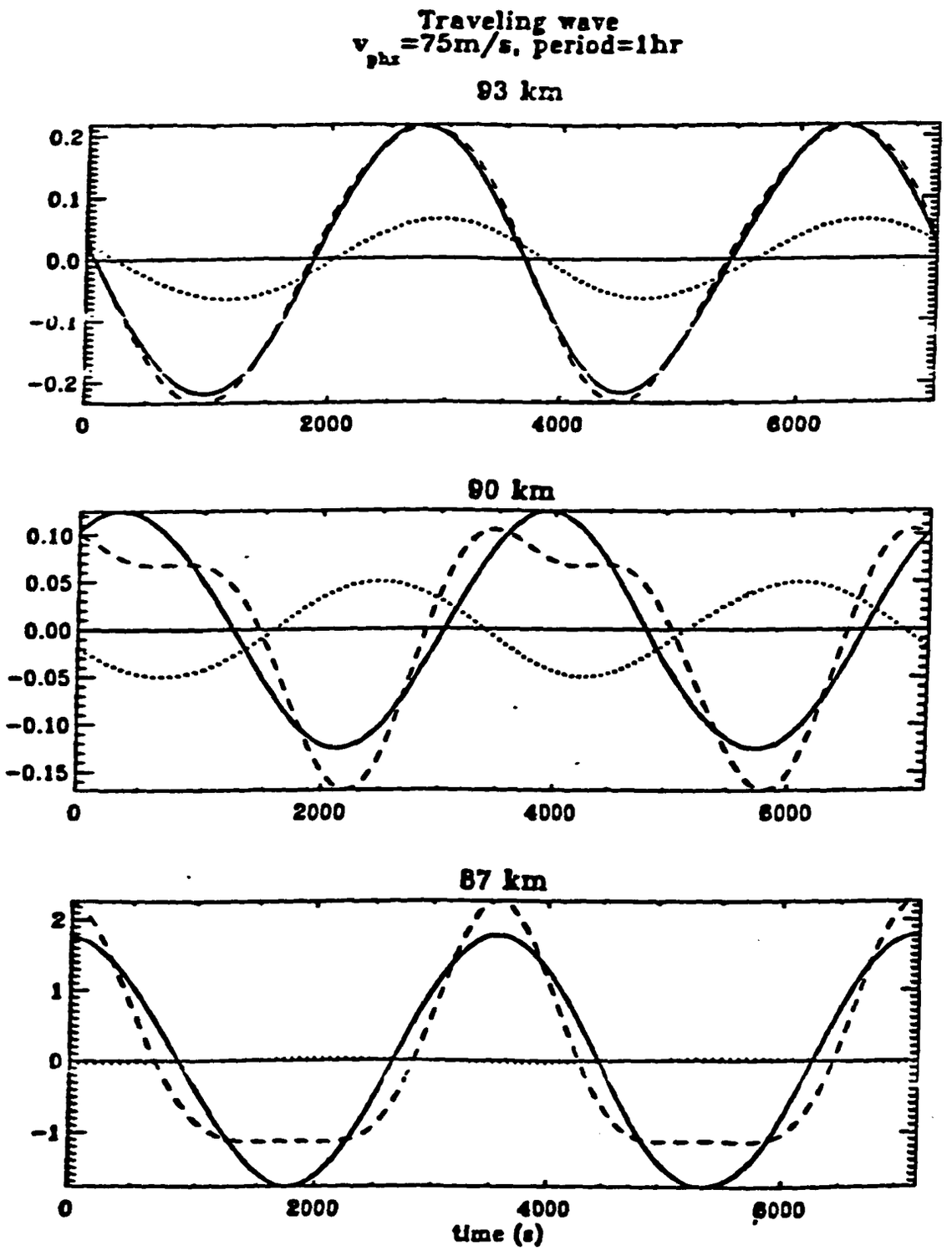

Fig. 3.3

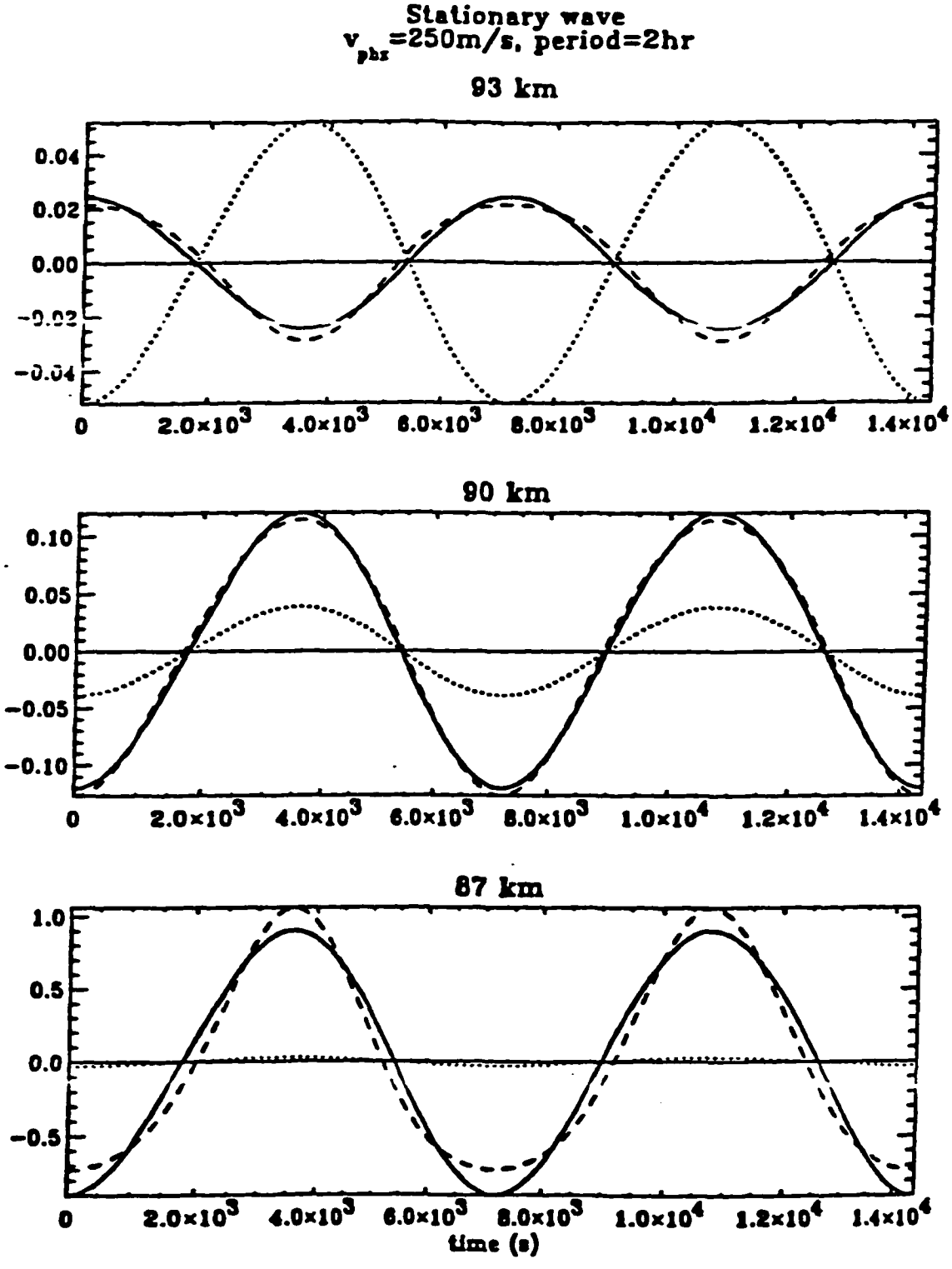

Fig. 3.4

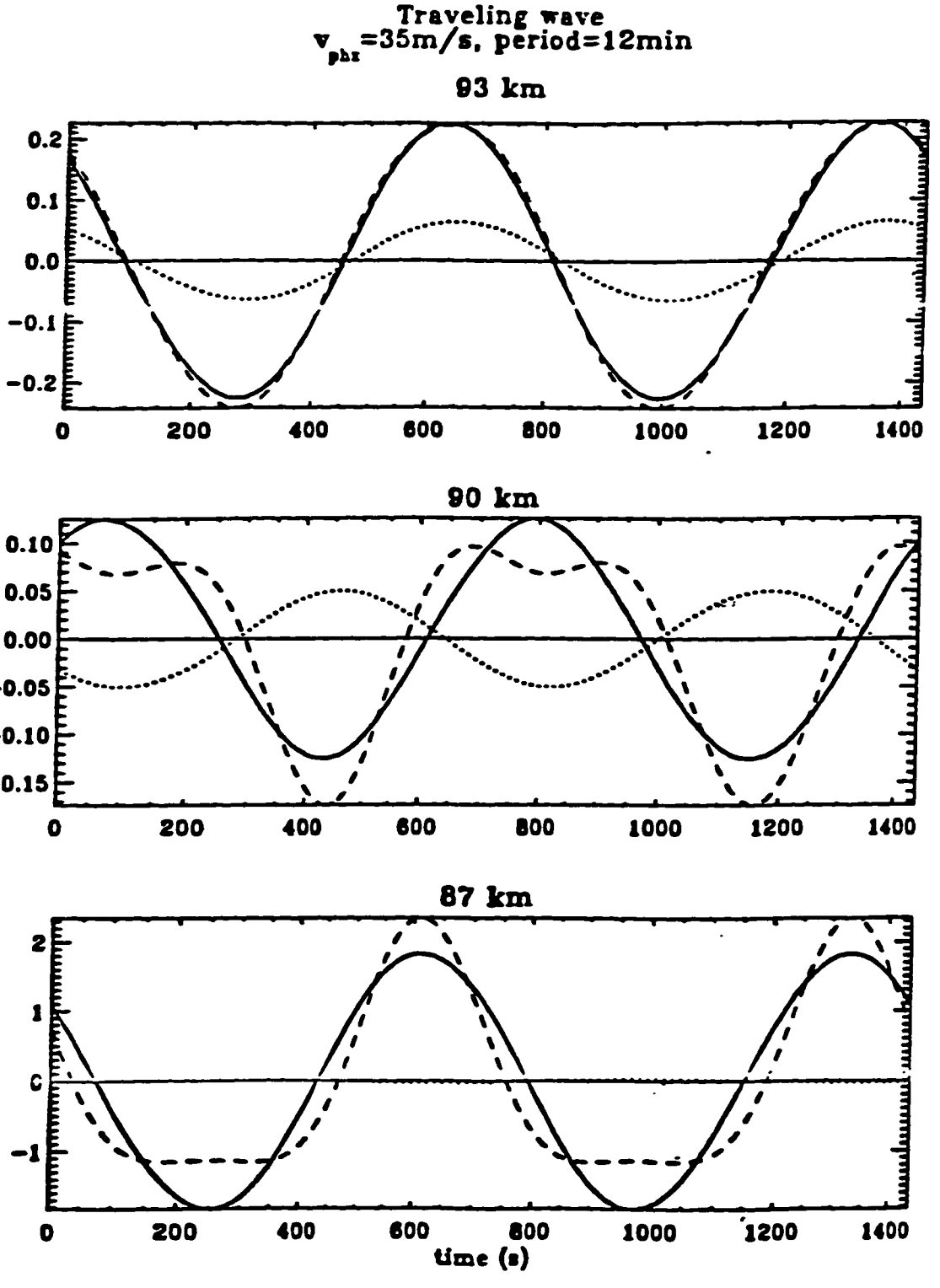

Fig. 3.5

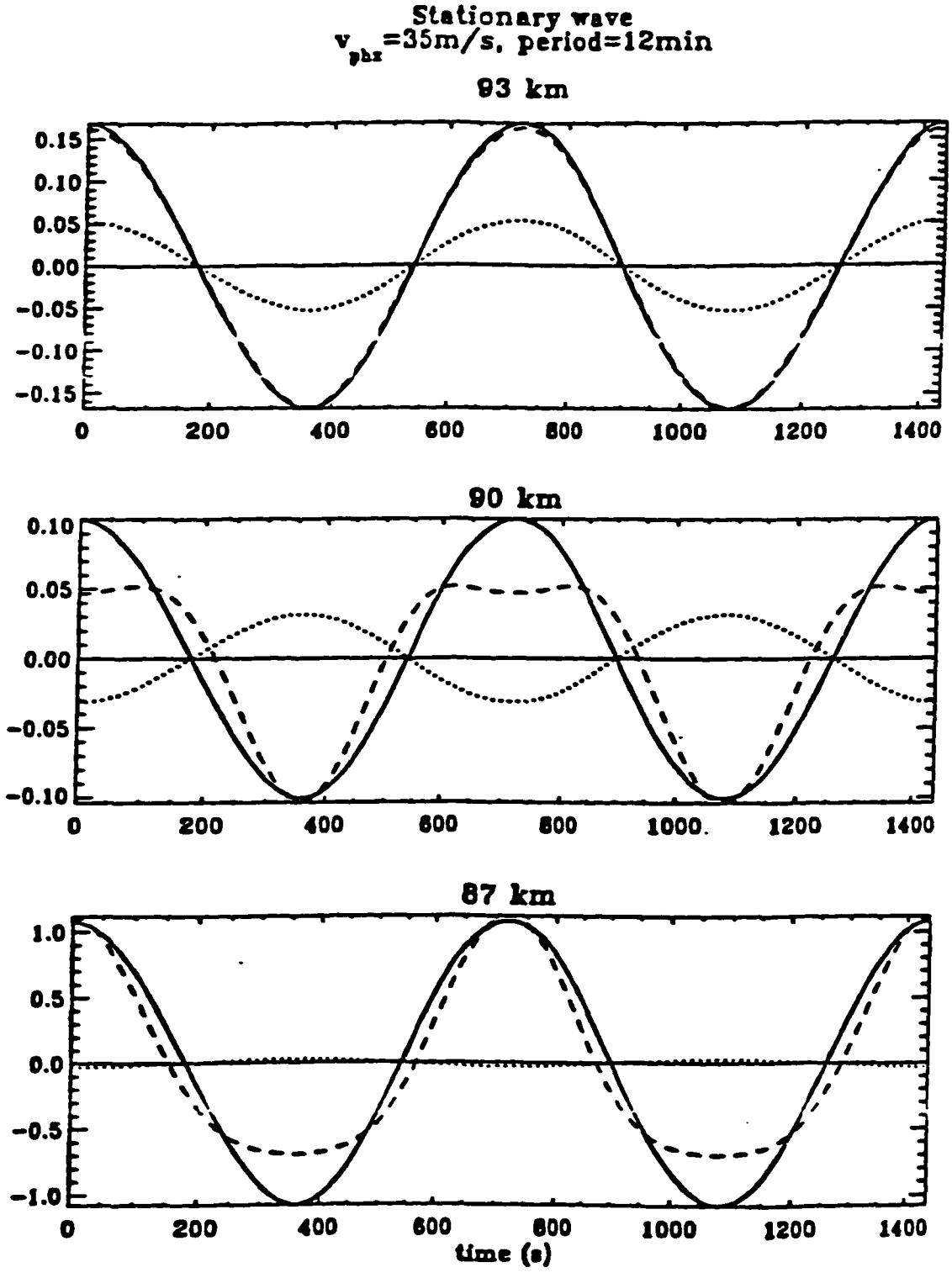

Fig. 3.6